

1 **Alzheimer's Disease Patient Brain Extracts Induce Multiple Pathologies in**  
2 **Vascularized Neuroimmune Organoids for Disease Modeling and Drug Discovery**

3

4 Yanru Ji<sup>1</sup>, Xiaoling Chen<sup>2</sup>, Meek Connor Joseph<sup>1</sup>, Jenna Lillie McLean<sup>1</sup>, Yang Yang<sup>2</sup>, Chongli  
5 Yuan<sup>3</sup>, Jean-Christophe Rochet<sup>2</sup>, Fei Liu<sup>4</sup>, Ranjie Xu<sup>1,\*</sup>

6

7 <sup>1</sup>Department of Basic Medical Sciences, College of Veterinary Medicine, Purdue University,  
8 West Lafayette, IN 47907

9 <sup>2</sup>Department of Medicinal Chemistry and Molecular Pharmacology, College of Pharmacy,  
10 Purdue University, West Lafayette, IN, 47907, USA

11 <sup>3</sup>Davidson School of Chemical Engineering, Purdue University, West Lafayette, IN 47907,  
12 USA

13 <sup>4</sup>Department of Neurochemistry, Inge Grundke-Iqbali Research Floor, New York State  
14 Institute for Basic Research in Developmental Disabilities, 1050 Forest Hill Road, Staten  
15 Island, NY 10314, USA

16

17 \*Address correspondence to:

18 Ranjie Xu, Ph.D.

19 Assistant Professor

20 Department of Basic Medical Sciences

21 Purdue University

22 625 Harrison St., West Lafayette, IN 47907

23 Email: [xu1726@purdue.edu](mailto:xu1726@purdue.edu)

24 Phone: 765-496-4007

25

26

27

28

29

30

31

32

33

1 **Abstract**

2 Alzheimer's Disease (AD) is the most common cause of dementia afflicting 55 million  
3 individuals worldwide, with limited treatment available. Current AD models mainly focus  
4 on familial AD (fAD), which is due to genetic mutations. However, models for studying  
5 sporadic AD (sAD), which represents over 95% of AD cases without specific genetic  
6 mutations, are severely limited. Moreover, the fundamental species differences between  
7 humans and animals might significantly contribute to clinical failures for AD therapeutics  
8 that have shown success in animal models, highlighting the urgency to develop more  
9 translational human models for studying AD, particularly sAD. In this study, we developed a  
10 complex human pluripotent stem cell (hPSC)-based vascularized neuroimmune organoid  
11 model, which contains multiple cell types affected in human AD brains, including human  
12 neurons, microglia, astrocytes, and blood vessels. Importantly, we demonstrated that brain  
13 extracts from individuals with sAD can effectively induce multiple AD pathologies in  
14 organoids four weeks post-exposure, including amyloid beta (A $\beta$ ) plaques-like aggregates,  
15 tau tangles-like aggregates, neuroinflammation, elevated microglial synaptic pruning,  
16 synapse/neuronal loss, and impaired neural network. Furthermore, after treatment with  
17 Lecanemab, an FDA-approved drug targeting A $\beta$ , AD brain extract exposed organoids  
18 showed a significant reduction of amyloid burden. Thus, the neuroimmune organoid model  
19 provides a unique opportunity to study AD, particularly sAD under a pathophysiological  
20 relevant three-dimensional (3D) human cell environment. It also holds great promise to  
21 facilitate AD drug development, particularly for immunotherapies.

22 **Keywords:** Sporadic Alzheimer's Disease; hPSC; organoids; Amyloid; tau; inflammation;  
23 microglia; Lecanemab; immunotherapy

24

1 **Introduction:**

2 Alzheimer's Disease (AD) is a devastating neurodegenerative disorder and the most  
3 common cause of dementia, affecting more than 55 million individuals globally[1, 2].  
4 Despite extensive efforts, most therapeutics have failed in clinical trials till now, with only  
5 limited effective treatments currently available[3-5]. AD is manifested with progressive  
6 cognitive decline and is characterized by multiple pathological hallmarks, including  
7 extracellular amyloid beta (A $\beta$ ) plaques, intracellular microtubule-associated tau  
8 neurofibrillary tangles (NFTs), neuroinflammation, synapse/neuronal loss, and brain  
9 atrophy[2, 4, 6]. To understand the mechanisms and develop therapeutics for AD, various  
10 animal models have been developed and significantly advanced our understanding of the  
11 disease mechanism[7-10]. However, most existing models focus on dominantly inherited  
12 familial AD (fAD), which is caused by genetic mutations in genes identified in individuals  
13 with fAD, including amyloid precursor protein (APP), presenilin1 (PSEN1), and presenilin2  
14 (PSEN2)[7, 10, 11]. In contrast, models for sporadic AD (sAD), which do not involve highly  
15 penetrating genetic mutations and account for 95% of all AD cases, are severely limited[3,  
16 10]. While both fAD and sAD share similar pathological hallmarks, such as A $\beta$  plaques and  
17 NFTs, the etiology of sAD is still largely unknown and may involve more complicated  
18 genetic and environmental interactions[9, 10]. Thus, developing appropriate models for  
19 sAD without genetic mutations is critically needed. Moreover, significant species difference  
20 exists between humans and rodents. For instance, many repeat sequences in the genome  
21 and gene splicing patterns are unique to humans[12]. These species differences may have  
22 profound impacts when modeling neurological disorders, particularly for AD, and may  
23 significantly contribute to the failures of many AD therapeutics that succeeded in pre-  
24 clinical animal studies but failed in clinical trials[3, 8, 13]. Therefore, it is critical to use  
25 human samples and develop human AD models that could recapitulate sAD features to  
26 advance our understanding of the disease mechanism and facilitate the development of  
27 therapeutic interventions.

28 Given the challenge of accessing and manipulating functional human brain tissues, human  
29 pluripotent stem cells (hPSCs), which include human embryonic stem cells (hESCs) and  
30 induced pluripotent stem cells (iPSCs), have emerged as valuable tools to utilize human  
31 cells for studying human neurological disorders, including AD[3, 14, 15]. The hPSC-based  
32 *in vitro* models, including two-dimensional (2D) and 3D models with pure human neural  
33 cells, are easy to manipulate and enable a high throughput for screening making them  
34 valuable for modeling AD[3, 16-18]. The hPSC 2D model is useful for dissecting the impact  
35 of genetic and other factors on the individual cell types involved in AD at a basic functional  
36 level[19-27]. On the other hand, recent studies have also highlighted the value of hPSC 3D

1 models, such as brain organoids and multiple cell type co-culture-based models, which  
2 incorporate various neural cell types and intricate cell-cell and cell-matrix interactions and  
3 preliminary neural structures, offering a more physiologically relevant environment to  
4 model diverse aspects of AD[28-36]. For example, fAD iPSC-derived brain organoids have  
5 successfully replicated AD pathological events, including A $\beta$  aggregates and  
6 hyperphosphorylated tau, and facilitated the understanding of AD, such as the roles of  
7 APOE4 and C3 complement in AD[28, 30, 33, 34].

8 However, critical limitations persist, impeding these 3D models from effectively modeling  
9 AD. (1) Most research used simple organoids composed mainly of neurons and astrocytes.  
10 Although some studies have integrated microglia into organoids, or incorporated blood  
11 vessels into 3D neural culture, it is still a challenge to integrate multiple cell types,  
12 particularly microglia and blood vessels simultaneously within one organoid to reflect the  
13 complex pathophysiological environment of AD brains. (2) The current organoid models for  
14 AD study mainly focused on fAD, and these models usually take three to six months to  
15 exhibit AD pathologies[30, 34, 35, 37]. An intriguing recent study induced sAD-like  
16 phenotypes by exposing healthy organoids to serum to mimic the condition of blood-brain  
17 barrier (BBB) leakage, a risk factor for sAD[36]. However, a brain organoid model that  
18 contains multiple cell types affected in AD brains, capable of effectively recapitulating key  
19 AD pathological hallmarks of sAD within a relatively short time frame induced by an  
20 efficient trigger for modeling sAD, is still lacking.

21 To circumvent these limitations, in this study, we developed a vascularized neuroimmune  
22 organoid model for studying AD, particularly for sAD. This organoid model contains  
23 multiple cell types that are affected in human AD brains, including human neurons,  
24 astrocytes, microglia, and blood vessels. Since AD postmortem brain tissues contain  
25 proteopathic seeds, including A $\beta$  and tau, that have the prion-like seeding activity to induce  
26 counterpart normal protein aggregate in animal models[38-42], we hypothesize that sAD  
27 postmortem tissues-derived brain extracts that contain both A $\beta$  and tau seeds, can induce  
28 multiple AD pathologies in human cells in organoids, mirroring observations in sAD.  
29 Remarkably, our results demonstrated that organoids exposed to AD brain extracts  
30 successfully recapitulated multiple AD-like pathologies, including A $\beta$  plaque-like  
31 aggregates, tau tangle-like aggregates, neuroinflammation, elevated microglial synaptic  
32 pruning, synapse/neuronal loss, but not organoids treated with vehicle control.  
33 Furthermore, we validated our organoids for drug discovery using Lecanemab, an FDA-  
34 approved anti-A $\beta$  antibody for AD treatment, and observed a significant alleviation of A $\beta$   
35 burden after treatment in the organoids that have been exposed to AD brain extracts. Thus,

1 this vascularized neuroimmune organoid model presents a unique opportunity to study  
2 sAD and holds great promise to facilitate AD drug development.

3

4 **Results**

5 **Generation and characterization of vascularized neuroimmune organoids**

6 To develop a brain organoid model that contains major cell types affected in human AD  
7 brains, building upon our previously established microglia-containing brain organoid  
8 model[43], we aim to introduce blood vessels into these organoids and develop a  
9 vascularized neuroimmune organoid model by co-culture of hPSCs-derived neural  
10 progenitor cells (NPCs), primitive macrophage progenitors (PMPs), and vascular  
11 progenitors (VPs) under 3D condition. To achieve this goal, we first generated NPCs and  
12 PMPs following our previous studies[43-45] (**Figure 1A**). The identity of hPSCs-derived  
13 NPCs was confirmed by co-expression of neural progenitor cell markers, PAX6 and NESTIN.  
14 PMPs were confirmed by co-expression of CD235, a marker for YS primitive hematopoietic  
15 progenitors[43], and CD43, a marker for hematopoietic progenitor-like cells[43] (**Figure**  
16 **1B**). VPs were generated using a published protocol with slight modifications detailed in  
17 Materials and Methods[46]. To generate brain organoids, the initial number was calibrated  
18 and co-cultured at 30,000 for NPCs, 12,000 for PMPs, and 7,000 for VPs, based on our  
19 previous experience. These cells spontaneously assembled and formed organoids on day  
20 1. Subsequent culture of the organoids was supplemented with mitogen fibroblast growth  
21 factor (bFGF) for 5 days to promote cellular proliferation (referred to as proliferation stage).  
22 Thereafter, organoids were transitioned to a neural differentiation medium which contained  
23 neurotrophic factors, interleukin-34 (IL-34), vascular endothelial growth factor (VEGF), and  
24 other necessary supplements for long-term culture to support neuronal, microglial, and  
25 vascular maturation (referred to as Differentiation stage) (**Figure 1A**). To ensure genetic  
26 diversity and robustness of our findings, three different hPSC lines (two iPSC lines, and one  
27 hESC line) from healthy individuals were used to derive progenitor cells.

28 To visualize the formation of blood vessels in living organoids, we incorporated VPs from an  
29 additional GFP-expressing hESC line (CAGG line). This allows us to track the vascular  
30 lineage cells by GFP signal. Under live cell imaging, clear and distinct branching structures  
31 were revealed in organoids on day 12 of culture (**Figure 1C**, left panel). Organoid sections  
32 without immunostaining also displayed lumen-like structures (**Figure 1C**, middle panel,  
33 and **Figure S1**). We further stained organoids with CD31, an endothelial cell marker, and  
34 observed CD31-expressing cells in organoids. The results confirmed the establishment of  
35 vascular structures within organoids (**Figure 1C**, right panel). At day 12, ventricular zone-

1 like regions were seen in organoids, which contained PAX6+ progenitors and  $\beta$ III-Tubulin+  
2 immature neurons (**Figure 1D**), mimicking the proliferative region in the developing cortical  
3 brain. To confirm PMPs differentiate into microglia at the differentiation stage, we first  
4 examined the expression of CD45 at day 12, which is a marker for all nucleated  
5 hematopoietic cells[43]. CD45+ cells exhibited a relatively even spatial distribution in  
6 organoids (**Figure 1E**, left panel). Microglial identity was further confirmed by double  
7 staining of CD45 and IBA1, a canonical macrophage/microglia marker[43]. CD45 and IBA1  
8 double staining showed ramified morphology, indicating healthy and functional microglia  
9 residing in organoids (**Figure 1E**, right panel). Previous studies have shown that NPCs can  
10 mature into neuronal lineage cells, including neurons and astrocytes in brain organoids[43,  
11 47]. To confirm neural maturation in the organoids, we first stained MAP2, a marker for  
12 neuronal dendrite, and observed robust expression of MAP2 at Day 45 (**Figure 1F**),  
13 suggesting NPCs efficiently differentiated into neurons. Further staining with NeuN, a  
14 mature neuron marker, and S100 $\beta$ , an astrocyte marker, revealed robust NeuN+ cells and  
15 S100 $\beta$ + cells, demonstrating that NPCs differentiated into mature neurons and astrocytes  
16 during the differentiation stage (**Figure 1G**). Taken together, we successfully developed  
17 vascularized neuroimmune organoids incorporating mature neurons, microglia, and  
18 vascular networks, which allows us to model the complex human brain environment.

19 **Sporadic AD (sAD) patient-derived brain extracts induce amyloid pathology in  
20 organoids**

21 Our next aim is to enable the vascularized neuroimmune organoids to efficiently  
22 recapitulate key AD pathological features for studying sAD without genetic mutations. Prior  
23 studies have shown that human misfolded proteopathic seeds, such as A $\beta$  or tau, can  
24 induce corresponding pathologies in transgenic mice engineered to express these human  
25 proteins[38-42]. Notably, recent studies suggested that A $\beta$  seeds may also be able to  
26 transmit among humans, for instance, individuals who received A $\beta$  contaminated cadaver-  
27 derived pituitary growth hormone (c-hGH) during childhood developed A $\beta$  pathologies and  
28 cerebral amyloid angiopathy (CAA) later in their life[48-50]. Based on these findings, we  
29 hypothesized that AD individual-derived brain extracts that contain proteopathic seeds,  
30 including A $\beta$  or tau, will induce AD pathologies in organoids as seen in human AD brains. To  
31 test our hypothesis and model sAD, we treated organoids with sAD individual postmortem  
32 tissue-derived brain extracts (henceforth, the AD group) to model sAD. The corresponding  
33 vehicle (buffer) was used as control (henceforth, the vehicle group). In addition, age-  
34 matched healthy individual-derived brain extracts were also included. Organoids after 10  
35 days of neuronal differentiation were exposed to AD brain extracts or the vehicle for two  
36 days, and samples were collected at 2 weeks or 4 weeks post-exposure. Subsequently, we

1 examined AD pathological hallmark expression, including A $\beta$  and tau pathologies,  
2 inflammation, and synapse/neuronal loss in organoids (**Figure 2A**).  
3 To examine A $\beta$  pathology characterized by extracellular A $\beta$  aggregates in organoids, we  
4 utilized 6E10 and 4G8 antibodies, which can detect the amino acid residues 3-8 or 17-24 of  
5 A $\beta$ , respectively[51]. Two weeks post brain extract or vehicle exposure, a modest number of  
6 weakly diffuse 6E10 and 4G8 signals were detected in both the AD and vehicle groups  
7 (**Figures 2B and S2**). Interestingly, only the AD group exhibited intraneuronal A $\beta$  aggregates,  
8 as indicated by the presence of discrete, punctate 6E10 signals around nuclei (**Figure 2B**,  
9 top panel). To exclude the possibility that aggregates were caused by other components  
10 contained in the brain extracts other than toxic protein seeds, age-matched healthy  
11 individual-derived brain extracts were included as the healthy control group. Similar to the  
12 vehicle group, diffuse but not aggregated signals were observed in healthy control brain  
13 extract-treated organoids (**Figure S3**). Since 6E10 can detect both A $\beta$  and intraneuronal  
14 amyloid precursor protein (APP)[51], the diffuse 6E10 and 4G8 signals might represent the  
15 endogenous APP. To confirm the presence of intraneuronal A $\beta$  aggregates in the AD group,  
16 we stained organoids with MOAB-2 antibody, which can specifically label intraneuronal A $\beta$ ,  
17 but not APP[51]. MOAB-2-expressing cells were only detected in the AD group, confirming  
18 the formation of intraneuronal A $\beta$  aggregates (**Figure S4**).  
19 Remarkably, after 4 weeks post AD brain extract exposure, multiple dense extracellular  
20 plaque-like aggregates were detected in the AD group but not the vehicle group(**Figure 2B**)  
21 or healthy control brain extract treated organoids (**Figure S3**). These extracellular  
22 aggregates were consistently identified in the AD group by 4G8 staining (**Figure 2C**).  
23 Quantitative analysis showed that compared to the vehicle group, the AD group  
24 demonstrates a significant escalation of A $\beta$  burden, as indicated by the positive areas of  
25 6E10 (AD vs Vehicle,  $1.24 \pm 0.28$  vs  $0.21 \pm 0.03$ ) and 4G8 (AD vs Vehicle,  $0.78 \pm 0.20$  vs  $0.13 \pm 0.02$ ) (**Figure 2D**). To confirm the composition of extracellular A $\beta$  aggregates, we  
27 performed double staining of organoids with 6E10 with another antibody A $\beta$ 42, which  
28 primarily targets A $\beta$ 42[52]. The overlapped punctate signals of 6E10 and A $\beta$ 42 were  
29 observed from extracellular regions in the AD group, suggesting that extracellular A $\beta$   
30 aggregates contain A $\beta$ 42 (**Figure 2E**). Moreover, to assess A $\beta$  plaque formation, we  
31 conducted double staining of organoids with 6E10 with a dye, Thioflavin-S, which binds to  
32  $\beta$ -sheet structure in protein aggregates, including plaques and tangles[53]. Consistently,  
33 the vehicle group showed some diffuse intraneuronal 6E10 signals, which were Thioflavin-S  
34 negative; only the AD group exhibited the co-localization of strong extracellular 6E10 and  
35 Thioflavin-S signals, reinforcing the presence of plaque-like aggregates in AD group (**Figure**  
36 **2F**, top panel). Collectively, these findings demonstrated that AD brain extracts containing

1 proteopathic A $\beta$  seeds can induce A $\beta$  pathology, including A $\beta$  plaque-like aggregates, in  
2 healthy brain organoids within a 4-week post-exposure time frame.

3 **Sporadic AD (sAD)patient-derived Brain extracts induce tau pathology in organoids**

4 Tau pathology, caused by the abnormal accumulation of the microtubule-associated  
5 protein tau, is a major pathological hallmark of AD. In human AD brains, tau undergoes  
6 abnormal hyperphosphorylation and other modifications, which convert it into a  
7 pathological protein with prion-like seeding activity and form neurofibrillary tangles  
8 (NFTs)[54, 55]. Given that the AD brain extracts applied in this study contained tau seeds  
9 (**Figure S5**), we wonder whether the AD brain extract can induce tau pathology in our  
10 organoid model. To examine tau pathology, we utilized a widely used antibody, AT8 that can  
11 detect phosphorylated tau[41]. Notably, 2 weeks post-exposure, the AD group presented  
12 with puncta-like, AT8-positive intraneuronal signals (**Figure 3A**, top panel), potentially  
13 indicating the formation of aggregates in neurons. Notably, 4 weeks post-AD brain extract  
14 exposure, the intensity and quantity of condensed AT8 signals increased significantly,  
15 suggesting further formation of tau aggregates (**Figure 3A**, top panel). In contrast, the  
16 vehicle group displayed no such phosphorylated tau aggregates at either time point (**Figure**  
17 **3A**, bottom panel), nor did healthy control brain extract treated organoids (**Figure S6**).  
18 Additionally, different from the condensed AT8 signals after AD brain extract exposure,  
19 weak and diffuse axonal AT8 positive signals were observed in organoids at 2 weeks post-  
20 exposure to the vehicle and healthy control brain extracts (**Figure 3A, S6, and S7**), aligning  
21 with prior studies that identified transient phosphorylated tau in neurons during  
22 development [48, 56].

23 Confirmation of tau aggregate was further achieved through Thioflavin-S and AT8 co-  
24 staining, which marked Thioflavin-S+ and AT-8+ double-positive cells exclusively in the AD  
25 group (**Figure 3B**). Quantification revealed a substantial increase in AT8-positive areas in  
26 the AD group compared to the vehicle group (AD vs Vehicle,  $0.88 \pm 0.15$  vs  $0.10 \pm 0.04$ )  
27 (**Figure 3C**), suggesting that AD brain extract was sufficient to induce tau pathology in  
28 organoids. To further confirm the formation of tau tangle-like structures, we performed  
29 Gallyas Silver Staining, a commonly used method for detecting tau tangles[57], and  
30 observed the formation of NFT-like structures in the AD group at four weeks post-exposure  
31 (**Figure 3D**). In all, our findings demonstrated that sAD brain extract can successfully  
32 induce tau pathology, including tau tangle-like aggregates, in healthy brain organoids.

33 **The AD neuroimmune organoids recapitulate neuroinflammation, phagocytosis of A $\beta$ ,**  
34 **and excessive microglial synaptic pruning**

1 In the AD environment, accumulating amyloid aggregates trigger the activation of microglia  
2 and astrocytes, and stimulate neuroinflammation by releasing inflammatory factors[58-  
3 60]. Since neuroimmune organoids contain microglia and astrocytes, to determine whether  
4 neuroimmune organoids can replicate neuroinflammation in AD brains, we measured the  
5 mRNA expression of the pro-inflammatory cytokine, IL-6, and chemokine, CCL2, by qRT-  
6 PCR in the organoids at four to six weeks post the exposure of AD brain extracts or vehicle  
7 treatments. As shown in **Figure 4A**, compared to the vehicle group, the AD group exhibits a  
8 significant increase in mRNA levels of IL-6 (AD vs. Vehicle,  $5.68 \pm 0.37$  vs.  $1.03 \pm 0.03$ ) and  
9 CCL2 (AD vs. Vehicle,  $1.46 \pm 0.10$  vs.  $1.01 \pm 0.01$ ), demonstrating that AD neuroimmune  
10 organoids recapitulated neuroinflammation. In addition, microglia play a beneficial role in  
11 AD by phagocytosis and removal A $\beta$ . To examine whether microglia in the AD group display  
12 this function, we conducted double staining of organoids with 6E10 and IBA1. 3D-  
13 reconstructive images from the Imaris software confirmed microglial engulfment of A $\beta$  in  
14 the AD group, aligning with previous evidence of microglial involvement in A $\beta$  clearance in  
15 AD[61, 62] (**Figure 4B**).

16 One significant detrimental role of microglia in AD is the abnormal removal of synaptic  
17 materials[63]. We subsequently evaluated whether human microglia in AD neuroimmune  
18 organoids could recapitulate this phenomenon. Organoids were stained with CD45 and  
19 Homer1 (a post-synaptic marker) at four weeks post-exposure to AD brain extracts or  
20 vehicles. The 3D-reconstructed images revealed that microglia pruned synaptic materials  
21 (**Figure 4C**). Quantification of the volume of Homer1 puncta within the volume of CD45  
22 indicated a significant increase of microglial pruning in the AD group (AD vs. Vehicle.,  $5.08$   
23  $\pm 0.9$  vs.  $1.00 \pm 0.18$ ) (**Figure 4D**). In summary, our results indicated that neuroimmune  
24 organoids can recapitulate neuroinflammation, as well as dynamic microglial functions in  
25 an AD-like 3D environment, which mirrors *in vivo* human microglia behaviors in the  
26 presence of AD pathologies.

27 **The AD neuroimmune organoids recapitulate synapse/ neuronal loss and impaired  
28 neural activity**

29 Synapse/neuronal loss is the key feature of AD[6, 64] and AD animal models are often  
30 limited to recapitulating neuronal loss[65-67]. To investigate whether brain organoids  
31 challenged by AD brain extracts could recapitulate this process, we first examined synaptic  
32 integrity by staining organoids with Homer1. Quantitative analysis of the number of  
33 Homer1 puncta per  $2500 \mu\text{m}^2$  revealed a reduction in the AD group (AD vs. Vehicle,  $1336.30$   
34  $\pm 92.93$  vs.  $6013.48 \pm 449.32$ ) (**Figures 5A and 5B**), indicating synapse loss in the AD group.  
35 Subsequently, we stained organoids with active Caspase3 to assess neuronal death in

1 organoids. Compared to the vehicle group, a significant increase in active Caspase3-  
2 expressing cells was detected in the AD group, demonstrating elevated neuronal death in  
3 the AD group (AD vs Vehicle,  $14.11 \pm 2.18$  vs  $2.66 \pm 0.17$ ) (**Figures 5C and 5D**).  
4 To further understand whether synapse/neuronal loss causes functional defects, we  
5 assessed the neural activity in the organoids employing MEA assay (**Figures 5E to 5G**).  
6 Spontaneous neural activities were recorded and analyzed in organoids that were seeded  
7 on electrodes and cultured for two additional weeks after four weeks post-AD brain extract  
8 or vehicle treatment. Our data revealed a reduced number of spikes, mean firing rate, and  
9 number of bursts in the AD group (**Figure 5H**), suggestive of impaired neural activity in the  
10 AD group. Together, these results indicated an environment conducive to synapse/neuronal  
11 loss, accompanied by compromised neural activity in AD neuroimmune organoids.

## 12 **Anti-A $\beta$ antibody Lecanemab relieved amyloid burden in AD neuroimmune organoids**

13 Since AD organoids can recapitulate AD pathologies, we wonder whether the organoid  
14 model could be used for AD drug discovery. Lecanemab, an FDA-approved humanized  
15 monoclonal A $\beta$  antibody for treating early AD, targets and neutralizes toxic A $\beta$ , facilitating  
16 their clearance from the brain[68-70]. Given that our organoids displayed A $\beta$  pathology  
17 after four weeks of AD brain extract exposure, we treated these neuroimmune organoids  
18 with Lecanemab for 2 consecutive weeks to evaluate their efficacy in our organoids.  
19 Staining with 6E10 and 4G8 post-treatment indicated that Lecanemab alleviated the  
20 amyloid burden in AD organoids (**Figures 6A and 6B**). It has been suggested that  
21 Lecanemab may induce phagocytosis and removal of A $\beta$  by microglia in human brains[71,  
22 72]. Therefore, we investigated the involvement of microglia in Lecanemab-mediated A $\beta$   
23 clearance in our organoids. Through staining with 6E10 and IBA1 and subsequent  
24 observation via 3D reconstructive images, we noted that microglia appeared to phagocytize  
25 A $\beta$  in the organoids. Interestingly, Lecanemab-treated organoids exhibited increased  
26 phagocytosis of A $\beta$  (**Figures 6C and 6D**). Overall, our results suggested that Lecanemab  
27 could relieve the A $\beta$  burden in AD organoids, which might involve phagocytosis of A $\beta$  by  
28 microglia. Consequently, our organoids demonstrated potential as a promising *in vitro*  
29 platform for testing AD therapeutics.

30

## 31 **Discussion**

32 Effectively modeling sAD to recapitulate multiple pathologies and developing platforms for  
33 drug discovery, have been challenged due to the complexity of the disease and the  
34 significant species differences between human and animal models. In this study, we  
35 presented a novel vascularized neuroimmune organoid model composed of human

1 neurons, astrocytes, microglia, and blood vessels. Upon exposure to sAD individual-  
2 derived extracts, the organoid successfully recapitulated multiple pathological features in  
3 sAD, including A $\beta$  plaque-like aggregates, neurofibrillary tangle-like aggregates,  
4 neuroinflammation, microglial synaptic pruning, synapse/neuronal loss, and impaired  
5 neural network. Furthermore, by validating the FDA-approved anti-A $\beta$  antibody Lecanemab,  
6 the organoid model demonstrates its potential as a platform for *in vitro* AD drug  
7 development, particularly for immunotherapies.

8 In contrast to other hiPSC-based AD brain organoid models, our vascularized  
9 neuroimmune organoid model has significant advantages to enable us to more efficiently  
10 model AD and test AD therapeutics. **(1)** The new organoid model incorporates multiple key  
11 cell types that are affected in human AD brains under a pathophysiological relevant 3D  
12 human cell-centric environment. Our organoid simultaneously includes neurons,  
13 astrocytes, microglia, and vasculatures, which enables a more comprehensive  
14 understanding of cell-cell interactions and cell-type-associated pathological events in AD,  
15 such as neuroinflammation and microglial synaptic pruning, which are absent in most AD  
16 organoid models (**Figure 4**). **(2)** The new organoid model can effectively develop multiple  
17 AD pathologies within a relatively short time frame, suitable for studying AD, particularly  
18 sAD. Previous AD organoid models were usually derived from fAD iPSC lines, which need  
19 long-term culture to replicate the AD pathologies. For instance, previous studies indicated  
20 that it took at least 5 months to exhibit amyloid plaque-like and neurofibrillary tangles-like  
21 aggregates[34], or 90 days to observe A $\beta$  aggregates and hyperphosphorylated tau  
22 protein[29], in fAD iPSC-derived brain organoids. Additionally, a recent study using healthy  
23 iPSC lines-derived organoids to model sAD through serum exposure required 3 to 4 months  
24 of culture to recapitulate A $\beta$  aggregates and hyperphosphorylated tau [36]. However, in our  
25 organoids, 4 weeks post-exposure to AD brain extracts, we successfully recapitulated  
26 multiple relatively mature AD pathologies, including A $\beta$  plaques-like aggregates and tau  
27 tangles-like aggregates, neuroinflammation, synapse/neuronal loss, in around 1.5-month-  
28 old organoids. This suggests that AD brain extracts can serve as a strong trigger to induce  
29 AD pathologies for studying AD, particularly sAD. In addition, complex cell types,  
30 particularly microglia and related neuroinflammation, absent in the previously mentioned  
31 organoids, may also contribute to efficiently recapitulating the AD pathologies in our  
32 organoids. With a similar strategy, it is possible to efficiently model fAD by exposing fAD-  
33 derived brain extracts to fAD iPSC-derived organoids. **(3)** The new organoid model is useful  
34 to serve as an *in vitro* platform to advance AD drug development, particularly antibody-  
35 based therapeutics (**Figure 6**), because the organoids contain microglia and can efficiently

1 recapitulate multiple AD pathologies, and microglia are expected to be a major cell  
2 component to degrade the antibody-binding protein aggregates, such as A $\beta$ .

3 Our results demonstrate that AD brain extracts can efficiently induce multiple AD  
4 pathologies in organoids, particularly A $\beta$  and tau pathologies. To induce AD pathologies, we  
5 utilized brain extracts from sAD individual postmortem brain tissues and hypothesized that  
6 the A $\beta$  and tau seeds in the brain extracts could induce multiple pathologies. As expected,  
7 post-exposure to sAD brain extracts, brain organoids can efficiently recapitulate A $\beta$  and tau  
8 pathologies. We first observed intraneuronal A $\beta$  accumulation, as indicated by punctate-  
9 like high-intensity 6E10-positive signals (**Figure 2B**), at 2 weeks postAD brain extract  
10 exposure. By the fourth week, these accumulations had progressed to extracellular A $\beta$   
11 plaque-like structures, indicated by the colocalization of 6E10 and Thioflavin-S (**Figures**  
12 **2B, 2C, and 2F**), suggesting a developing pattern from intraneuronal aggregation to  
13 extracellular deposition. This pattern is in line with the findings in AD and Down Syndrome  
14 individuals, where intraneuronal amyloid aggregates were found in brain regions vulnerable  
15 to dementia, such as the hippocampus and entorhinal cortex, preceding the formation of  
16 extracellular plaques[73-77]. Similarly, organoids demonstrated puncta-like aggregates of  
17 hyperphosphorylated tau 2 weeks post AD brain extract exposure and exhibited tangle-like  
18 structures by the fourth week post-exposure, indicated by the Thioflavin-S and Gallyas  
19 Silver Staining (**Figures 3 A, 3B, and 3D**).

20 On the other hand, our results provide direct evidence that proteopathic seeds, not only A $\beta$   
21 but tau, can spread among human cells and tissue-like 3D structures, and induce AD-like  
22 A $\beta$  and tau pathologies. This aligns with the clinical observations that A $\beta$  contaminated c-  
23 hGH can cause A $\beta$  pathologies and CAA in humans over decades[49, 50, 58]. This also  
24 corroborates the concept of the prion-like property of AD proteopathic proteins and the  
25 possible transmission of AD between humans by accidents in medical or surgical  
26 procedures, raising the awareness to prevent iatrogenic human transmission of AD.

27 Neuroinflammation and synapse/neuronal loss are known to appear along the progression  
28 of AD[78]. In the early stages of the disease, stimuli like extracellular A $\beta$  activate  
29 neuroinflammatory responses that may recruit microglia for A $\beta$  clearance[58, 59].  
30 Consistent with this, in our organoids, mRNA expression levels of inflammatory cytokines  
31 in the AD group (**Figure 4A**). Furthermore, A $\beta$  signals were detected inside of microglia,  
32 indicating microglial phagocytosis and clearance of A $\beta$  in organoids (**Figure 4B**).  
33 Additionally, align with previous studies showing that excessive microglia-mediated  
34 synaptic pruning in AD animal models [63, 79], we observed a significant microglia  
35 synaptic removal (**Figures 4C, 4D**), and a significant synaptic materials decrease in AD

1 organoids (**Figures 5 A and 5B**). Additionally, elevated neuronal death was confirmed by  
2 activated Caspase3 signaling increment in the AD group (**Figures 5 C and 5D**). Although  
3 studies have found neuronal hyperactivity in the presence of amyloid beta pathology, *in*  
4 *vivo* research has proved that tau dominated A $\beta$  when both were present in transgenic mice  
5 models[80]. In agreement with these observations, our MEA assay of organoids revealed  
6 impaired neuronal networks (**Figures 5E to 5H**), with fewer spikes and bursts recorded  
7 compared to the vehicle group, corroborating previous research findings.

8 The neuroimmune organoids, containing multiple cell types (including microglia) and  
9 exhibiting AD-like pathologies, are particularly valuable for testing AD therapeutics,  
10 especially immunotherapies. The recent FDA-approved anti-A $\beta$  monoclonal antibody,  
11 Lecanemab, underscores the tremendous potential of antibody-based immunotherapies  
12 for tackling AD[5, 81, 82]. However, species differences may hinder the translational  
13 efficacy of preclinical animal models in clinical trials, highlighting the urgent need for  
14 human models to test these immunotherapies before clinical trials. **(1)** Recent cryo-EM  
15 findings have uncovered species-specific aggregate structures of proteopathic proteins in  
16 AD[83]. Aggregate structures observed in AD animal models are often not present in  
17 individuals with AD[84]. This discrepancy potentially impedes our assessment of the  
18 efficacy of the therapeutics and contributes to translation failures. **(2)** Antibodies-based  
19 therapeutics targeting toxic proteins, such as targeting A $\beta$ , are usually tested in animals.  
20 Before moving to clinical trials, successful antibody candidates undergo a humanization  
21 process to avoid immune rejection, such as by replacing the murine IgG with the human  
22 version [85]. However, the humanization process may substantially compromise the  
23 efficacy of the antibodies and even cause side effects[86]. Thus, direct testing of these  
24 human antibodies in human models is crucial. **(3)** Antibody-targeted protein aggregates,  
25 such as Lecanemab-binding A $\beta$  protofibrils, are hypothesized to be recognized and  
26 removed by microglia, the immune cells in the brain[70-72]. However, there are no suitable  
27 human models available that can recapitulate AD pathologies and contain human  
28 microglia for directly testing these human versions of antibody-based therapeutics. Our  
29 organoids contain multiple cell types, including microglia, and develop AD-like pathologies  
30 that offer a unique platform to solve this limitation. To assess whether our organoid model  
31 could serve as an ideal *in vitro* platform for testing AD drugs, we validated Lecanemab in  
32 our organoids. Following a 4-week post-exposure to AD brain extracts, we treated our AD  
33 organoids with Lecanemab for two weeks and observed a significant decrease in amyloid  
34 burden. Notably, we also observed an increased microglial engulfment of A $\beta$  in the  
35 Lecanemab-treated group (**Figure 6**), providing direct evidence that human microglia  
36 involved the Lecanemab-mediated A $\beta$  removal.

1 While the inclusion of blood vessels improves the overall health of the organoids to better  
2 model the complexity of the brain environment, we did not detect the presence of CAA,  
3 where A $\beta$  fibrils are deposited along the cerebral vasculatures, a common vascular  
4 pathology in AD[64]. This may require an extended culture period post-AD extract exposure.  
5 In addition, a critical challenge for iPSC-based brain organoid models is the relatively  
6 immature state of human cells[87]. Recent studies, including ours, have developed  
7 chimeric brain models by transplanting iPSC-derived organoids or neural cells into animal  
8 brains, where human cells can survive and mature as animals age under the conducive  
9 physiological *in vivo* environment[44, 45, 88, 89]. It will be promising to transplant our  
10 organoids into animal brains and test whether our organoids can better model AD features  
11 in the context of aged human cells within the host brain in the future. Overall, our  
12 innovative vascularized neuroimmune organoids present unique opportunities to model  
13 sAD and advance drug discovery for AD.

14

## 15 **Material and Methods**

### 16 **Culture and quality control of hPSC lines**

17 Three different hiPSC lines, KOLF2.1, ND2, and GCaMP, as well as one hESC cell line  
18 CAGG, were used in this study (**Supplementary Table S1**). The hiPSCs were maintained  
19 under feeder-free condition and cultured on hESC-qualified Matrigel (Corning) coated dish  
20 in mTeSR plus media (STEMCELL Technologies). The hiPSCs were passaged at  
21 approximately 70% confluence with ReLeSR media (STEMCELL Technologies).

22

### 23 **pNPC generation and culture**

24 Small molecule-based protocols were applied when generating pNPCs as in our previous  
25 studies[45, 90]. Neural differentiation in the embryoid bodies (EBs) was induced by dual  
26 inhibition of SMAD signaling. In summary, EBs were cultured in neural induction medium  
27 composed of DMEM/F12 (HyClone) and 1  $\times$  N2 Supplement (Thermo Fisher Scientific)  
28 supplied with inhibitor SB431542 (2  $\mu$ M, Stemgent) and noggin (50 ng/mL, Peprotech) for 6  
29 days before plating on growth factor-reduced Matrigel (BD Biosciences) coated plates. EBs  
30 were cultured with neural induction medium supplied with laminin (1  $\mu$ g/mL, Corning) for 7  
31 days, and then pNPCs in the form of neural rosette were manually isolated from  
32 surrounding cells. Isolated pNPCs were expanded for 5 to 7 days, depending on the  
33 confluence, in pNPC medium, which is composed of a 1:1 mixture of Neurobasal (Thermo  
34 Fisher Scientific) and DMEM/F12, supplemented with 1 $\times$ N2, 1 $\times$ B27-RA (Thermo Fisher  
35 Scientific), FGF2 (20 ng/mL, Peprotech), human leukemia inhibitory factor (hLIF, 10 ng/mL,

1 Millipore), CHIR99021 (3  $\mu$ M, Biogems), SB431542 (2  $\mu$ M), and ROCK inhibitor Y-27632 (10  
2  $\mu$ M, Tocris).

3

4 **PMP generation and culture**

5 PMPs were generated as previous studies[44, 91]. Briefly, embryoid bodies (EBs) were  
6 generated from hiPSCs and induced to yolk sac EBs (YS-EBs) by adding bone  
7 morphogenetic protein 4 (BMP4, 50 ng/mL, Peprotech; to induce mesoderm), vascular  
8 endothelial growth factor (VEGF, 50 ng/mL, Peprotech; endothelial precursors), and stem  
9 cell factor (SCF, 20 ng/mL, Miltenyi Biotech; Hematopoietic precursors) into mTeSR1 media  
10 (STEMCELL Technologies) for 5 days. Next, YS-EBs were plated into dishes and cultured  
11 with PMP medium composed of interleukin-3 (IL-3, 25 ng/mL, Peprotech) and macrophage  
12 colony-stimulating factor (M-CSF, 100ng/mL, Peprotech) in XVIVO media (Lonza). Human  
13 PMPs emerged into the supernatant 2 to 3 weeks after plating and were continuously  
14 produced for more than 3 months.

15

16 **VP generation and culture**

17 VPs were generated using a published protocol with minor modifications[46]. In brief,  
18 hiPSCs were dissociated to form aggregates in a low-attachment plate and differentiated  
19 into mesoderm with CHIR99021 (12  $\mu$ M, Peprotech) and BMP4 (30 ng/mL) in a 1:1 mixture  
20 of Neurobasal and DMEM/F12, supplemented with 1 $\times$ N2, 1 $\times$ B27-RA for 3 days. Then,  
21 vascular lineage induction was performed with VEGF (100 ng/mL) and forskolin (2  $\mu$ M) for 2  
22 days. Cell aggregates were then embedded into growth factor-reduced Matrigel, cultured  
23 with VEGF (100 mg/mL), FGF2 (100 ng/mL), and 15% FBS (Gibco) in XVIVO media for 5 days  
24 to allow vessel sprouting. Cell aggregates were dissociated by TrypLE into single cells,  
25 which served as the VP for the following organoid generation.

26

27 **Brain extract preparation and tau seeding activity confirmation**

28 To obtain 10% (w/v) brain extracts, frozen temporal cortex tissues of histopathologically  
29 confirmed AD cases with Braak Stages V-VI from the Brain Tissue Resource Center, McLean  
30 Hospital, Belmont, MA, USA, were prepared in homogenization buffer (20 mM Tris-HCl, pH  
31 8.0, 0.32 M sucrose, 10 mM $\beta$ -mercaptoethanol ( $\beta$ -ME), 5 mM MgSO<sub>4</sub>, 1 mM EDTA, 10 mM  
32 glycerophosphate, 1 mM Na<sub>3</sub>VO<sub>4</sub>, 50 mM NaF, 2 mM benzamidine, 1 mM 4-(2-aminoethyl)  
33 benzenesulfonyl fluoride hydrochloride (AEBSF), and 10  $\mu$ g/ml each aprotinin, leupeptin,  
34 and pepstatin), and centrifuged at 10,000 $\times$ g for 30 min, as previously reported[92, 93]. Tau  
35 seeding activity of brain extracts was confirmed (**Figure S5**), using *in vitro* seeded tau  
36 aggregation assay, in which HEK-293T cells expressing HA-tau<sub>151-391</sub> was treated with brain

1 extracts and lysed in RIPA buffer. Seeded HA-tau<sub>151-391</sub> aggregates were yielded by  
2 ultracentrifugation and analyzed by immuno-blots, as previously reported[92, 93].  
3

4 **Organoid assembly, culture, brain extract treatment, and drug treatment**

5 To generate vascularized immune-brain organoids, 30,000 pNPCs, 12,000 PMPs, and 7,000  
6 VPs were co-cultured for organoid self-assembly. Organoids were cultured in a 1:1 mixture  
7 of NPC medium (1:1 mixture of Neurobasal and DMEM/F12, supplemented with 1×N2,  
8 1×B27-RA, FGF2 (20 ng/mL) and PMP medium for 5 days to allow proliferation, and were  
9 transferred to ND medium, which is composed of a 1:1 mixture of Neurobasal and  
10 DMEM/F12, supplemented with 1×N2, 1×B27-RA, BDNF (10 ng/mL, Peprotech), GDNF (10  
11 ng/mL, Peprotech), L-Ascorbic acid (200 nM, Sigma Aldrich), c-AMP (1 μM, Sigma Aldrich),  
12 IL-34 (100 ng/mL, Peprotech), M-CSF (25 ng/mL), TGF-β1 (50 ng/mL, Peprotech). After 10  
13 days of differentiation, vehicle or brain extracts derived from AD patients, or age-matched  
14 healthy individuals (10 μL/mL), were added to medium for two days. The organoids were  
15 collected at 2 weeks or 4 weeks post-exposure to brain extracts or the vehicle. Four weeks  
16 post exposure to brain extracts, Lecanemab (Sellekchem, Cat#A3112) was added to  
17 medium at a concentration of 10 mg/mL. Samples were collected after 2 weeks of  
18 Lecanemab treatment.  
19

20 **Immunohistochemistry and cell counting**

21 Organoids were fixed with 4% paraformaldehyde and then cryo-sectioned at 15 μm  
22 thickness for immunostaining. The tissues were blocked with a blocking solution (5% goat  
23 or donkey serum in PBS with 0.2% Triton X-100) at room temperature for 1 hr. Primary  
24 antibodies were diluted in the same blocking solution and incubated at 4 °C overnight.  
25 Sections were washed with PBS and incubated with secondary antibodies for 1 hr at room  
26 temperature. Sections were then washed with PBS and were mounted with anti-fade  
27 Fluoromount-G medium containing 1,4,6-diamidino-2-phenylindole dihydrochloride  
28 (DAPI) (Southern Biotechnology). Antibodies used were listed in **Supplementary Table S2**.  
29 For Thioflavin-S staining, sections were washed with 70% and 80% ethanol for 1 minute,  
30 respectively, followed by 15 minutes of incubation of 0.05% freshly prepared and filtered  
31 Thioflavin-S solution. Samples were then washed with 80% and 70% ethanol sequentially  
32 for 1 minute, and finally rinsed with water. Images were captured with a Zeiss LSM 900  
33 confocal microscopy. Image analysis was performed using Fiji (NIH). Relative fluorescence  
34 intensity was presented as normalized value to the vehicle group. Cells, plaques, or  
35 synapses were counted with Fiji. At least three fields of each organoid were chosen

1 randomly to count after Z projection. The data are repeated three to four times (n=3 or 4)  
2 from 3 hPSC lines, each experiment used one hPSC line and contained 4-6 organoids.  
3

4 **Gallyas Silver Staining**

5 The Gallyas silver staining method was used to stain the Tau tangles (57), details are  
6 included in Supplementary materials. Slides were washed in distilled water for one minute  
7 and transferred immediately to alkali silver iodide for 15 minutes. Next, slides were washed  
8 for 1 minute in 2% oxalic acid, followed by three washes in distilled water for 1 minute.  
9 Then the slides were incubated in alkaline silver iodide solution for 2-5 minutes followed by  
10 three rinsing in 0.5% acetic acid for 1 minute each. Then slides were incubated in physical  
11 developer solution for 15 -20 minutes. The developer was made fresh before use in a 1:1  
12 ratio (solution A: solution B). Next, the samples were washed in 0.5% acetic acid and 1%  
13 sodium thiosulfate for 5 minutes each. Subsequently, samples were washed in distilled  
14 water for five minutes, and incubated in 0.5% gold chloride solution, and sodium  
15 thiosulfate for 5 minutes each. Finally, the samples were washed in distilled water for five  
16 minutes, counterstained with nuclear fast red, and mounted using Permount solution.  
17

18 **RNA isolation and qPCR**

19 Total RNA isolation was performed with TRIzol Reagent (Invitrogen) and complementary  
20 DNA was prepared with SuperScript IV First-Strand Synthesis System (Invitrogen)[94]. The  
21 qPCR assays were performed with SYBR Green PCR Master Mix in QuantStudio 3 (Applied  
22 Biosystems), primers used were listed in **Supplementary Table S3**[95]. The  $2^{-\Delta\Delta Ct}$  method  
23 was used to calculate relative gene expression after normalization to the  $\beta$ -actin internal  
24 control.  
25

26 **Microelectrode Arrays (MEA)**

27 Organoids at around 21 days were seeded into 48-well transparent MEA plates (Axion  
28 Biosystems) at one organoid per well. MEA assays were performed with Maestro Pro  
29 platform (Axion Biosystems) and recorded using AxIS software. Organoids were fed with  
30 BrainPhys media (STEMCELL Technologies) supplemented with 1×N2, 1×B27, 20 ng/mL  
31 BDNF, 20 ng/mL GDNF, as well as brain extract or vehicle. For recording, following a 5 min  
32 resting time in the instrument, each plate was recorded for 10 min to calculate the spike  
33 per well. Experiments were repeated for four times, each experiment used one hPSC line  
34 and contained 3-4 organoids. MEA analysis was performed using the Axion Biosystems  
35 NeuralMetrics Tool.  
36

1 **Statistics and reproducibility**

2 All data represent mean  $\pm$  SEM. Significance is determined using a two-tailed unpaired t-  
3 test with Welch's correction for comparing two independent groups, or a one-way ANOVA  
4 test with Bonferroni post-hoc test for comparing three or more groups. A p value  $< 0.05$  was  
5 considered significant. Analyses were performed with GraphPad Prism 10. All experiments  
6 were independently performed at least three times.

7

8 **Acknowledgments**

9 This work was in part supported by grants from the lab startup package, the Showalter  
10 grant, and the Purdue Institute for Integrative Neuroscience research grant (iPSC/Organoid  
11 Technologies) to X.R. We appreciate Ying Liu from Florida International University for  
12 providing ND2 iPSC and CAGG hESC lines in this study. We thank Xinqi Guo and Raymond  
13 Pan from the Xu Laboratory for their assistance with immunohistochemistry.

14

15 **Authors' contributions**

16 R.X. and J. Y designed the experiments and interpreted the data. J.Y. carried out most of the  
17 experiments with technical assistance from C. X., C.E., J.C.M, and L.F, prepared the brain  
18 extracts with quality control. C. X., and Y. Y assistance with MEA recording. L.F., R. JC., Y. C.,  
19 and Y. Y. provided critical suggestions. R.X. directed the project and wrote the manuscript  
20 together with J.Y. with input from all co-authors.

21

22 **Conflict of interest**

23 The authors declare that they have no conflict of interest.

24

25

26

27

28

29

30

31

32

33

34

35

36

37

38

39

1    **References**

- 3    1. *2022 Alzheimer's disease facts and figures*. Alzheimers Dement, 2022. **18**(4): p. 700-  
4    789.
- 5    2. Scheltens, P., et al., *Alzheimer's disease*. Lancet, 2021. **397**(10284): p. 1577-1590.
- 6    3. Scearce-Levie, K., P.E. Sanchez, and J.W. Lewcock, *Leveraging preclinical models*  
7    *for the development of Alzheimer disease therapeutics*. Nat Rev Drug Discov, 2020.  
8    **19**(7): p. 447-462.
- 9    4. Long, J.M. and D.M. Holtzman, *Alzheimer Disease: An Update on Pathobiology and*  
10   *Treatment Strategies*. Cell, 2019. **179**(2): p. 312-339.
- 11   5. Boxer, A.L. and R. Sperling, *Accelerating Alzheimer's therapeutic development: The*  
12   *past and future of clinical trials*. Cell, 2023. **186**(22): p. 4757-4772.
- 13   6. DeTure, M.A. and D.W. Dickson, *The neuropathological diagnosis of Alzheimer's*  
14   *disease*. Mol Neurodegener, 2019. **14**(1): p. 32.
- 15   7. Jankowsky, J.L. and H. Zheng, *Practical considerations for choosing a mouse model*  
16   *of Alzheimer's disease*. Mol Neurodegener, 2017. **12**(1): p. 89.
- 17   8. Dawson, T.M., T.E. Golde, and C. Lagier-Tourenne, *Animal models of*  
18   *neurodegenerative diseases*. Nat Neurosci, 2018. **21**(10): p. 1370-1379.
- 19   9. Vitek, M.P., et al., *Translational animal models for Alzheimer's disease: An*  
20   *Alzheimer's Association Business Consortium Think Tank*. Alzheimers Dement (N Y),  
21   2020. **6**(1): p. e12114.
- 22   10. Götz, J., L.G. Bodea, and M. Goedert, *Rodent models for Alzheimer disease*. Nat Rev  
23   Neurosci, 2018. **19**(10): p. 583-598.
- 24   11. Karch, C.M. and A.M. Goate, *Alzheimer's disease risk genes and mechanisms of*  
25   *disease pathogenesis*. Biol Psychiatry, 2015. **77**(1): p. 43-51.
- 26   12. Fisher, E.M.C. and D.M. Bannerman, *Mouse models of neurodegeneration: Know*  
27   *your question, know your mouse*. Science Translational Medicine, 2019. **11**(493): p.  
28   eaaq1818.
- 29   13. Fisher, E.M.C. and D.M. Bannerman, *Mouse models of neurodegeneration: Know*  
30   *your question, know your mouse*. Sci Transl Med, 2019. **11**(493).
- 31   14. Okano, H. and S. Morimoto, *iPSC-based disease modeling and drug discovery in*  
32   *cardinal neurodegenerative disorders*. Cell Stem Cell, 2022. **29**(2): p. 189-208.
- 33   15. Ji, Y., J.L. McLean, and R. Xu, *Emerging Human Pluripotent Stem Cell-Based Human-*  
34   *Animal Brain Chimeras for Advancing Disease Modeling and Cell Therapy for*  
35   *Neurological Disorders*. Neurosci Bull, 2024.
- 36   16. Penney, J., W.T. Ralvenius, and L.H. Tsai, *Modeling Alzheimer's disease with iPSC-*  
37   *derived brain cells*. Mol Psychiatry, 2020. **25**(1): p. 148-167.
- 38   17. Cerneckis, J., G. Bu, and Y. Shi, *Pushing the boundaries of brain organoids to study*  
39   *Alzheimer's disease*. Trends Mol Med, 2023. **29**(8): p. 659-672.
- 40   18. Blanchard, J.W., M.B. Victor, and L.H. Tsai, *Dissecting the complexities of Alzheimer*  
41   *disease with in vitro models of the human brain*. Nat Rev Neurol, 2022. **18**(1): p. 25-  
42   39.

- 1 19. Wang, C., et al., *Gain of toxic apolipoprotein E4 effects in human iPSC-derived*  
2 *neurons is ameliorated by a small-molecule structure corrector.* Nat Med, 2018.  
3 **24(5):** p. 647-657.
- 4 20. van der Kant, R., et al., *Cholesterol Metabolism Is a Druggable Axis that*  
5 *Independently Regulates Tau and Amyloid- $\beta$  in iPSC-Derived Alzheimer's Disease*  
6 *Neurons.* Cell Stem Cell, 2019. **24(3):** p. 363-375.e9.
- 7 21. Traxler, L., et al., *Warburg-like metabolic transformation underlies neuronal*  
8 *degeneration in sporadic Alzheimer's disease.* Cell Metab, 2022. **34(9):** p. 1248-  
9 1263.e6.
- 10 22. Mertens, J., et al., *Age-dependent instability of mature neuronal fate in induced*  
11 *neurons from Alzheimer's patients.* Cell Stem Cell, 2021. **28(9):** p. 1533-1548.e6.
- 12 23. Lin, Y.T., et al., *APOE4 Causes Widespread Molecular and Cellular Alterations*  
13 *Associated with Alzheimer's Disease Phenotypes in Human iPSC-Derived Brain Cell*  
14 *Types.* Neuron, 2018. **98(6):** p. 1141-1154.e7.
- 15 24. Lagomarsino, V.N., et al., *Stem cell-derived neurons reflect features of protein*  
16 *networks, neuropathology, and cognitive outcome of their aged human donors.*  
17 *Neuron, 2021. 109(21):* p. 3402-3420.e9.
- 18 25. Kwart, D., et al., *A Large Panel of Isogenic APP and PSEN1 Mutant Human iPSC*  
19 *Neurons Reveals Shared Endosomal Abnormalities Mediated by APP  $\beta$ -CTFs, Not*  
20  *$\mathcal{A}\beta$ .* Neuron, 2019. **104(2):** p. 256-270.e5.
- 21 26. Kondo, T., et al., *Modeling Alzheimer's disease with iPSCs reveals stress phenotypes*  
22 *associated with intracellular  $\mathcal{A}\beta$  and differential drug responsiveness.* Cell Stem  
23 *Cell, 2013. 12(4):* p. 487-96.
- 24 27. Israel, M.A., et al., *Probing sporadic and familial Alzheimer's disease using induced*  
25 *pluripotent stem cells.* Nature, 2012. **482(7384):** p. 216-20.
- 26 28. Zhao, J., et al., *APOE4 exacerbates synapse loss and neurodegeneration in*  
27 *Alzheimer's disease patient iPSC-derived cerebral organoids.* Nat Commun, 2020.  
28 **11(1):** p. 5540.
- 29 29. Sun, Z., et al., *Endogenous recapitulation of Alzheimer's disease neuropathology*  
30 *through human 3D direct neuronal reprogramming.* bioRxiv, 2023.
- 31 30. Raja, W.K., et al., *Self-Organizing 3D Human Neural Tissue Derived from Induced*  
32 *Pluripotent Stem Cells Recapitulate Alzheimer's Disease Phenotypes.* PLoS One,  
33 **2016. 11(9):** p. e0161969.
- 34 31. Park, J., et al., *A 3D human triculture system modeling neurodegeneration and*  
35 *neuroinflammation in Alzheimer's disease.* Nat Neurosci, 2018. **21(7):** p. 941-951.
- 36 32. Huang, S., et al., *Chimeric cerebral organoids reveal the essentials of neuronal and*  
37 *astrocytic APOE4 for Alzheimer's tau pathology.* Signal Transduct Target Ther, 2022.  
38 **7(1):** p. 176.
- 39 33. Guttikonda, S.R., et al., *Fully defined human pluripotent stem cell-derived microglia*  
40 *and tri-culture system model C3 production in Alzheimer's disease.* Nat Neurosci,  
41 **2021. 24(3):** p. 343-354.

1 34. Gonzalez, C., et al., *Modeling amyloid beta and tau pathology in human cerebral*  
2 *organoids*. Mol Psychiatry, 2018. **23**(12): p. 2363-2374.

3 35. Choi, S.H., et al., *A three-dimensional human neural cell culture model of*  
4 *Alzheimer's disease*. Nature, 2014. **515**(7526): p. 274-8.

5 36. Chen, X., et al., *Modeling Sporadic Alzheimer's Disease in Human Brain Organoids*  
6 *under Serum Exposure*. Adv Sci (Weinh), 2021. **8**(18): p. e2101462.

7 37. Kwak, S.S., et al., *Amyloid- $\beta$ 42/40 ratio drives tau pathology in 3D human neural cell*  
8 *culture models of Alzheimer's disease*. Nat Commun, 2020. **11**(1): p. 1377.

9 38. Meyer-Luehmann, M., et al., *Exogenous induction of cerebral beta-amyloidogenesis*  
10 *is governed by agent and host*. Science, 2006. **313**(5794): p. 1781-4.

11 39. Kane, M.D., et al., *Evidence for seeding of beta -amyloid by intracerebral infusion of*  
12 *Alzheimer brain extracts in beta -amyloid precursor protein-transgenic mice*. J  
13 Neurosci, 2000. **20**(10): p. 3606-11.

14 40. Iba, M., et al., *Synthetic tau fibrils mediate transmission of neurofibrillary tangles in*  
15 *a transgenic mouse model of Alzheimer's-like tauopathy*. J Neurosci, 2013. **33**(3): p.  
16 1024-37.

17 41. Hu, W., et al., *Hyperphosphorylation determines both the spread and the*  
18 *morphology of tau pathology*. Alzheimers Dement, 2016. **12**(10): p. 1066-1077.

19 42. Clavaguera, F., et al., *Transmission and spreading of tauopathy in transgenic mouse*  
20 *brain*. Nat Cell Biol, 2009. **11**(7): p. 909-13.

21 43. Xu, R., et al., *Developing human pluripotent stem cell-based cerebral organoids*  
22 *with a controllable microglia ratio for modeling brain development and pathology*.  
23 Stem Cell Reports, 2021. **16**(8): p. 1923-1937.

24 44. Xu, R., et al., *Human iPSC-derived mature microglia retain their identity and*  
25 *functionally integrate in the chimeric mouse brain*. Nat Commun, 2020. **11**(1): p.  
26 1577.

27 45. Xu, R., et al., *OLIG2 Drives Abnormal Neurodevelopmental Phenotypes in Human*  
28 *iPSC-Based Organoid and Chimeric Mouse Models of Down Syndrome*. Cell Stem  
29 Cell, 2019. **24**(6): p. 908-926.e8.

30 46. Wimmer, R.A., et al., *Generation of blood vessel organoids from human pluripotent*  
31 *stem cells*. Nat Protoc, 2019. **14**(11): p. 3082-3100.

32 47. Reubinoff, B.E., et al., *Neural progenitors from human embryonic stem cells*. Nat  
33 Biotechnol, 2001. **19**(12): p. 1134-40.

34 48. Purro, S.A., et al., *Transmission of amyloid- $\beta$  protein pathology from cadaveric*  
35 *pituitary growth hormone*. Nature, 2018. **564**(7736): p. 415-419.

36 49. Jaunmuktane, Z., et al., *Evidence for human transmission of amyloid- $\beta$  pathology*  
37 *and cerebral amyloid angiopathy*. Nature, 2015. **525**(7568): p. 247-50.

38 50. Banerjee, G., et al., *Iatrogenic Alzheimer's disease in recipients of cadaveric*  
39 *pituitary-derived growth hormone*. Nat Med, 2024. **30**(2): p. 394-402.

40 51. Youmans, K.L., et al., *Intraneuronal A $\beta$  detection in 5xFAD mice by a new A $\beta$ -*  
41 *specific antibody*. Mol Neurodegener, 2012. **7**: p. 8.

1 52. Willén, K., et al., *A $\beta$  accumulation causes MVB enlargement and is modelled by*  
2 *dominant negative VPS4A*. Mol Neurodegener, 2017. **12**(1): p. 61.

3 53. Rajamohamedsait, H.B. and E.M. Sigurdsson, *Histological staining of amyloid and*  
4 *pre-amyloid peptides and proteins in mouse tissue*. Methods Mol Biol, 2012. **849**: p.  
5 411-24.

6 54. Iqbal, K., F. Liu, and C.X. Gong, *Tau and neurodegenerative disease: the story so far*.  
7 Nat Rev Neurol, 2016. **12**(1): p. 15-27.

8 55. Congdon, E.E., et al., *Tau-targeting therapies for Alzheimer disease: current status*  
9 *and future directions*. Nat Rev Neurol, 2023. **19**(12): p. 715-736.

10 56. Imbimbo, B.P., et al., *A critical appraisal of tau-targeting therapies for primary and*  
11 *secondary tauopathies*. Alzheimers Dement, 2022. **18**(5): p. 1008-1037.

12 57. Moloney, C.M., V.J. Lowe, and M.E. Murray, *Visualization of neurofibrillary tangle*  
13 *maturity in Alzheimer's disease: A clinicopathologic perspective for biomarker*  
14 *research*. Alzheimers Dement, 2021. **17**(9): p. 1554-1574.

15 58. Leng, F. and P. Edison, *Neuroinflammation and microglial activation in Alzheimer*  
16 *disease: where do we go from here?* Nat Rev Neurol, 2021. **17**(3): p. 157-172.

17 59. Kinney, J.W., et al., *Inflammation as a central mechanism in Alzheimer's disease*.  
18 Alzheimers Dement (N Y), 2018. **4**: p. 575-590.

19 60. Hansen, D.V., J.E. Hanson, and M. Sheng, *Microglia in Alzheimer's disease*. J Cell  
20 Biol, 2018. **217**(2): p. 459-472.

21 61. Lee, C.Y. and G.E. Landreth, *The role of microglia in amyloid clearance from the AD*  
22 *brain*. J Neural Transm (Vienna), 2010. **117**(8): p. 949-60.

23 62. Hickman, S.E., E.K. Allison, and J. El Khoury, *Microglial dysfunction and defective*  
24 *beta-amyloid clearance pathways in aging Alzheimer's disease mice*. J Neurosci,  
25 2008. **28**(33): p. 8354-60.

26 63. Hong, S., et al., *Complement and microglia mediate early synapse loss in Alzheimer*  
27 *mouse models*. Science, 2016. **352**(6286): p. 712-716.

28 64. Serrano-Pozo, A., et al., *Neuropathological alterations in Alzheimer disease*. Cold  
29 Spring Harb Perspect Med, 2011. **1**(1): p. a006189.

30 65. Morrisette, D.A., et al., *Relevance of transgenic mouse models to human Alzheimer*  
31 *disease*. J Biol Chem, 2009. **284**(10): p. 6033-7.

32 66. Kokjohn, T.A. and A.E. Rohr, *Amyloid precursor protein transgenic mouse models*  
33 *and Alzheimer's disease: understanding the paradigms, limitations, and*  
34 *contributions*. Alzheimers Dement, 2009. **5**(4): p. 340-7.

35 67. Espuny-Camacho, I., et al., *Hallmarks of Alzheimer's Disease in Stem-Cell-Derived*  
36 *Human Neurons Transplanted into Mouse Brain*. Neuron, 2017. **93**(5): p. 1066-  
37 1081.e8.

38 68. Vitek, G.E., B. Decourt, and M.N. Sabbagh, *Lecanemab (BAN2401): an anti-beta-*  
39 *amyloid monoclonal antibody for the treatment of Alzheimer disease*. Expert Opin  
40 *Investig Drugs, 2023. **32**(2): p. 89-94.*

41 69. van Dyck, C.H., M. Sabbagh, and S. Cohen, *Lecanemab in Early Alzheimer's*  
42 *Disease. Reply*. N Engl J Med, 2023. **388**(17): p. 1631-1632.

1 70. Qiao, Y., et al., *Safety and efficacy of lecanemab for Alzheimer's disease: a*  
2 *systematic review and meta-analysis of randomized clinical trials.* Front Aging

3 Neurosci, 2023. **15**: p. 1169499.

4 71. Tobeh, N.S. and K.D. Bruce, *Emerging Alzheimer's disease therapeutics: promising*  
5 *insights from lipid metabolism and microglia-focused interventions.* Front Aging

6 Neurosci, 2023. **15**: p. 1259012.

7 72. Cummings, J., et al., *Anti-Amyloid Monoclonal Antibodies for the Treatment of*  
8 *Alzheimer's Disease.* BioDrugs, 2024. **38**(1): p. 5-22.

9 73. D'Andrea, M.R., et al., *Evidence that neurones accumulating amyloid can undergo*  
10 *lysis to form amyloid plaques in Alzheimer's disease.* Histopathology, 2001. **38**(2): p.

11 120-34.

12 74. Brion, J.P., et al., *Developmental changes in tau phosphorylation: fetal tau is*  
13 *transiently phosphorylated in a manner similar to paired helical filament-tau*  
14 *characteristic of Alzheimer's disease.* J Neurochem, 1993. **61**(6): p. 2071-80.

15 75. Wegiel, J., et al., *Intraneuronal Abeta immunoreactivity is not a predictor of brain*  
16 *amyloidosis-beta or neurofibrillary degeneration.* Acta Neuropathol, 2007. **113**(4): p.

17 389-402.

18 76. Nagele, R.G., et al., *Intracellular accumulation of beta-amyloid(1-42) in neurons is*  
19 *facilitated by the alpha 7 nicotinic acetylcholine receptor in Alzheimer's disease.*  
20 Neuroscience, 2002. **110**(2): p. 199-211.

21 77. LaFerla, F.M., K.N. Green, and S. Oddo, *Intracellular amyloid-beta in Alzheimer's*  
22 *disease.* Nat Rev Neurosci, 2007. **8**(7): p. 499-509.

23 78. Thakur, S., et al., *Neuroinflammation in Alzheimer's Disease: Current Progress in*  
24 *Molecular Signaling and Therapeutics.* Inflammation, 2023. **46**(1): p. 1-17.

25 79. Rajendran, L. and R.C. Paolicelli, *Microglia-Mediated Synapse Loss in Alzheimer's*  
26 *Disease.* J Neurosci, 2018. **38**(12): p. 2911-2919.

27 80. Busche, M.A., et al., *Tau impairs neural circuits, dominating amyloid-β effects, in*  
28 *Alzheimer models in vivo.* Nat Neurosci, 2019. **22**(1): p. 57-64.

29 81. Jucker, M. and L.C. Walker, *Alzheimer's disease: From immunotherapy to*  
30 *immunoprevention.* Cell, 2023. **186**(20): p. 4260-4270.

31 82. Tabor, G.T. and D.M. Holtzman, *Current status of amyloid-targeting*  
32 *immunotherapies for Alzheimer's disease.* Sci Transl Med, 2023. **15**(721): p.

33 eadk9993.

34 83. Yang, Y., et al., *Cryo-EM structures of amyloid-β 42 filaments from human brains.*  
35 Science, 2022. **375**(6577): p. 167-172.

36 84. Zielinski, M., et al., *Cryo-EM of Aβ fibrils from mouse models find tg-APP(ArcSwe)*  
37 *fibrils resemble those found in patients with sporadic Alzheimer's disease.* Nat

38 Neurosci, 2023. **26**(12): p. 2073-2080.

39 85. Harding, F.A., et al., *The immunogenicity of humanized and fully human antibodies:*  
40 *residual immunogenicity resides in the CDR regions.* MAbs, 2010. **2**(3): p. 256-65.

41 86. Almagro, J.C., et al., *Progress and Challenges in the Design and Clinical*  
42 *Development of Antibodies for Cancer Therapy.* Front Immunol, 2017. **8**: p. 1751.

1 87. Andrews, M.G. and A.R. Kriegstein, *Challenges of Organoid Research*. Annu Rev  
2 Neurosci, 2022. **45**: p. 23-39.

3 88. Mansour, A.A., et al., *An in vivo model of functional and vascularized human brain*  
4 *organoids*. Nat Biotechnol, 2018. **36**(5): p. 432-441.

5 89. Revah, O., et al., *Maturation and circuit integration of transplanted human cortical*  
6 *organoids*. Nature, 2022. **610**(7931): p. 319-326.

7 90. Chambers, S.M., et al., *Highly efficient neural conversion of human ES and iPS cells*  
8 *by dual inhibition of SMAD signaling*. Nat Biotechnol, 2009. **27**(3): p. 275-80.

9 91. Haenseler, W., et al., *A Highly Efficient Human Pluripotent Stem Cell Microglia*  
10 *Model Displays a Neuronal-Co-culture-Specific Expression Profile and*  
11 *Inflammatory Response*. Stem Cell Reports, 2017. **8**(6): p. 1727-1742.

12 92. Zhou, Y., et al., *Relevance of Phosphorylation and Truncation of Tau to the*  
13 *Etiopathogenesis of Alzheimer's Disease*. Front Aging Neurosci, 2018. **10**: p. 27.

14 93. Li, L., et al., *Alzheimer's disease brain contains tau fractions with differential prion-*  
15 *like activities*. Acta Neuropathol Commun, 2021. **9**(1): p. 28.

16 94. Jin, M., et al., *Type-I-interferon signaling drives microglial dysfunction and*  
17 *senescence in human iPSC models of Down syndrome and Alzheimer's disease*.  
18 Cell Stem Cell, 2022. **29**(7): p. 1135-1153.e8.

19 95. Miao, L., et al., *Targeting the STING pathway in tumor-associated macrophages*  
20 *regulates innate immune sensing of gastric cancer cells*. Theranostics, 2020. **10**(2):  
21 p. 498-515.

22

23

24

25

26

27

28

29

30

31

32

33

1 **Figure legends:**

2 **Figure 1. Generation and characterization of vascularized neuroimmune organoids.**

3 (A) Schematic image of the generation of vascularized neuroimmune organoids. hPSCs-  
4 derived NPCs, PMPs, and VPs were co-cultured to form 3D spheroids. The proliferation  
5 stage lasted for five days before organoids were cultured in a differentiation medium. Scale  
6 bars, 750 or 300  $\mu$ m as indicated.

7 (B) Left panel, representatives of PAX6 $^+$  and NESTIN $^+$  NPCs. Right panel, CD235 $^+$  and CD43 $^+$   
8 PMPs. Scale bars, 20 or 10  $\mu$ m as indicated.

9 (C) Representatives of blood vessels in 12-day-old organoids. Left panel, CAGG-derived  
10 blood vessels in living organoids; Middle panel, sections of organoids incorporated with  
11 CAGG-derived blood vessels; Right panel, representative of CD31 staining. Scale bars, 300,  
12 100, or 20  $\mu$ m as indicated.

13 (D) Representative of neural rosette stained with PAX6 and  $\beta$ III-tubulin in 12-day-old  
14 organoids. Scale bar, 20  $\mu$ m.

15 (E) Characterization of microglia in 12-day-old organoids. Left panel, representative of  
16 CD45 $^+$  microglia; Right panel, representative of CD45 $^+$ Iba1 $^+$  microglia. Scale bars, 20, 10, or  
17 5  $\mu$ m as indicated.

18 (F) Representative of MAP2 expression in 45-day-old organoids. Scale bar, 50  $\mu$ m.

19 (G) Representatives of NeuN $^+$  neurons and S100 $\beta$  $^+$  astrocytes in 45-day-old organoids.  
20 Scale bar, 20  $\mu$ m.

21

22 **Figure 2. Sporadic AD patient-derived brain extracts induce amyloid pathology in  
23 organoids.**

24 (A) Schematic image of experimental design.

25 (B) Representatives of 6E10 in organoids at 2 or 4 weeks post-exposure to AD brain extracts  
26 or vehicle. Scale bars, 20 or 10  $\mu$ m as indicated.

27 (C) Representatives of 4G8 in organoids at 2 or 4 weeks post-exposure to AD brain extracts  
28 or vehicle. Scale bars, 20 or 10  $\mu$ m as indicated.

29 (D) Quantification of percentage area of 6E10 $^+$  signals and 4G8 $^+$  signals over time. n=4  
30 independent experiments from 3 hPSC lines, each experiment used one hPSC line and  
31 contained 4-6 organoids. Data are presented as mean  $\pm$  SEM. Unpaired t test with Welch's  
32 correction, \*p < 0.05, ns represents no significance.

33 (E) Representatives of co-staining with 6E10 and A $\beta$ 42 in organoids at 4 weeks post-  
34 exposure to AD brain extracts. Scale bars, 10 or 5  $\mu$ m as indicated.

35 (F) Representatives of Thioflavin-S $^+$  and 6E10 $^+$  structures in organoids at 4 weeks post-  
36 exposure to AD brain extracts or vehicle. Scale bar, 20  $\mu$ m.

1 **Figure 3. Sporadic AD patient-derived brain extracts induce tau pathology in  
2 organoids.**

3 (A) Representatives of AT8<sup>+</sup> cells in organoids at 2 or 4 weeks post-exposure to AD brain  
4 extracts or vehicle. Scale bars, 20 or 10  $\mu$ m as indicated.  
5 (B) Representatives of AT8 and Thioflavin-S labeled hyperphosphorylated tau aggregates in  
6 organoids at 4 weeks post-exposure to AD brain extracts. Scale bars, 20, 10, or 5  $\mu$ m as  
7 indicated.  
8 (C) Quantification of AT8 positive cells over time. n=4 independent experiments from 3  
9 hPSC lines, each experiment used one hPSC line and contained 4-6 organoids. Data are  
10 presented as mean  $\pm$  SEM. Unpaired t test with Welch's correction, \*p < 0.05, ns represents  
11 no significance.  
12 (D) Representatives of Gallyas silver staining of organoid at 4 weeks post-exposure to AD  
13 brain extracts or vehicle. Scale bar, 20  $\mu$ m.

14

15 **Figure 4. The AD neuroimmune organoids recapitulate neuroinflammation,  
16 phagocytosis of A $\beta$ , and excessive microglial synaptic pruning.**

17 (A) qPCR analysis of mRNA expression level of *IL-6* and *CCL2* in organoids from 4 to 6  
18 weeks post-exposure to AD brain extract or vehicle. n = 3 independent from two hPSCs  
19 lines, each experiment used one hPSC line and contained 4-6 organoids. Unpaired  
20 student's t test, \*p < 0.05, \*\*p < 0.01.  
21 (B) 3D reconstructive image showing microglia phagocytizing A $\beta$ . Organoid sections from  
22 the AD group treated with AD brain extracts were stained with IBA1 and 6E10. Scale bar, 2  
23  $\mu$ m.  
24 (C) 3D reconstructive image showing microglial synaptic pruning. Sections from organoids  
25 at 4 weeks post-exposure to the vehicle or AD brain extracts were stained with Homer1 and  
26 hCD45. Scale bars, 5 or 3  $\mu$ m as indicated.  
27 (D) Quantification of Homer1 puncta engulfment within CD45-positive microglia for the  
28 vehicle and AD groups. The phagocytic activity of microglia was quantified by dividing  
29 Homer1 puncta volume with microglia volume. n = 4 independent experiments from three  
30 hPSC lines, each experiment used one hPSC line and contained 4-6 organoids. Data are  
31 presented as mean  $\pm$  SEM. Unpaired t test with Welch's correction, \*\*\*p < 0.001. Scale  
32 bars, as indicated.

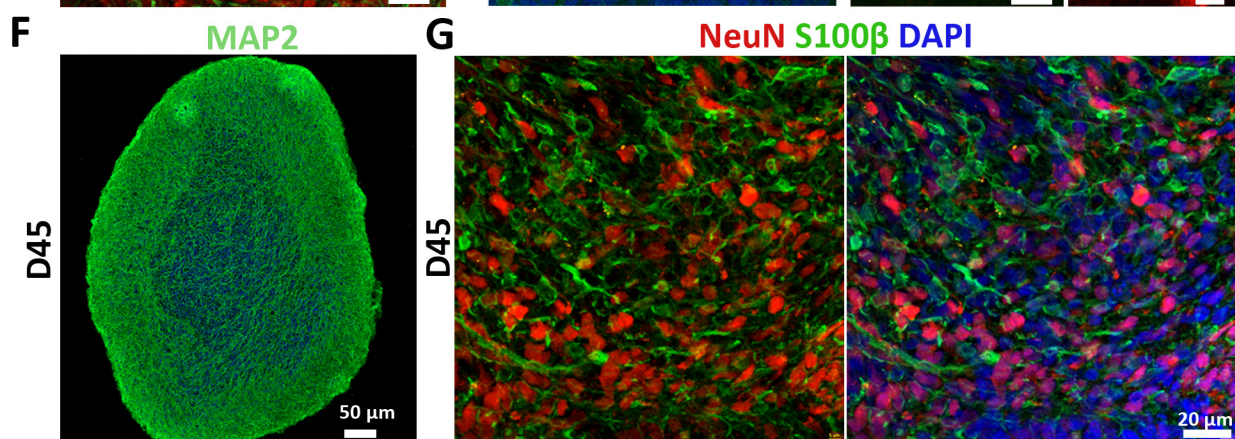
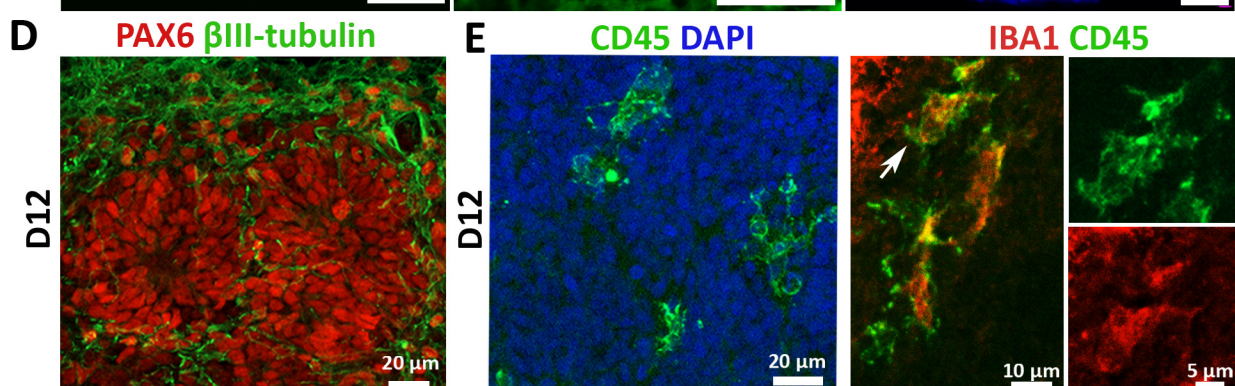
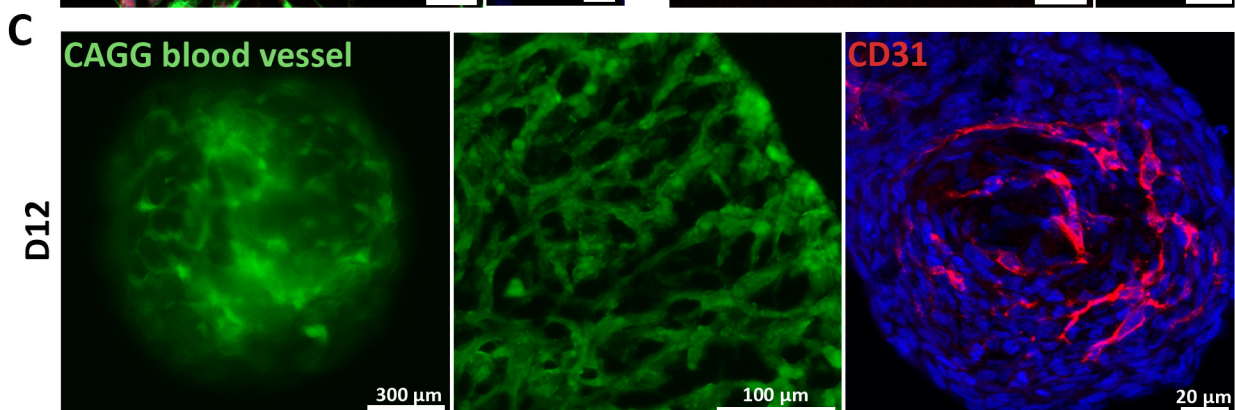
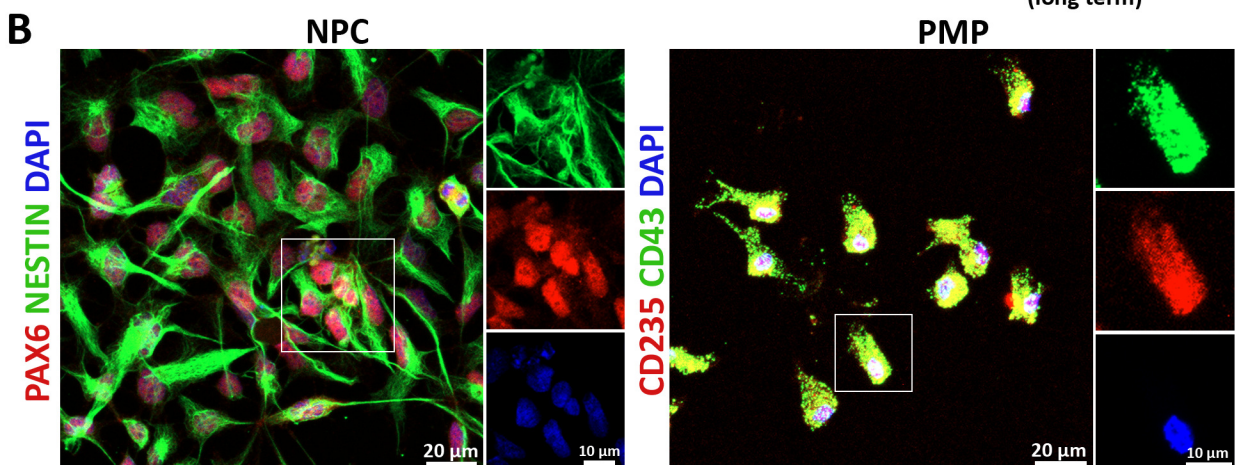
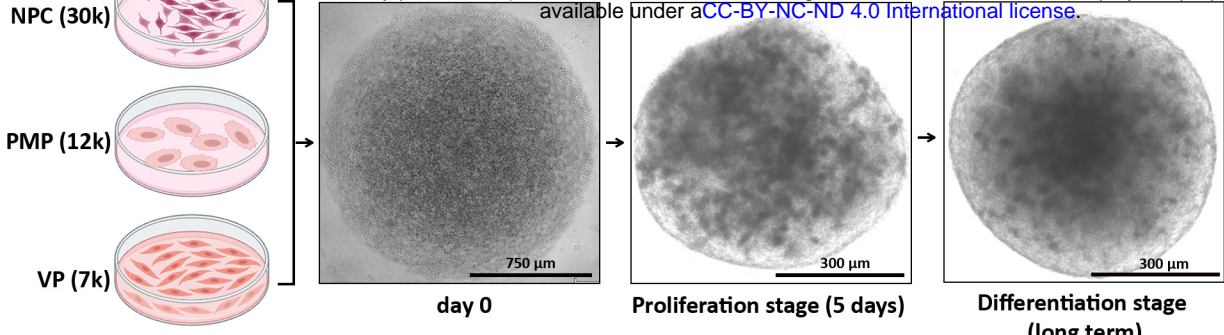
33

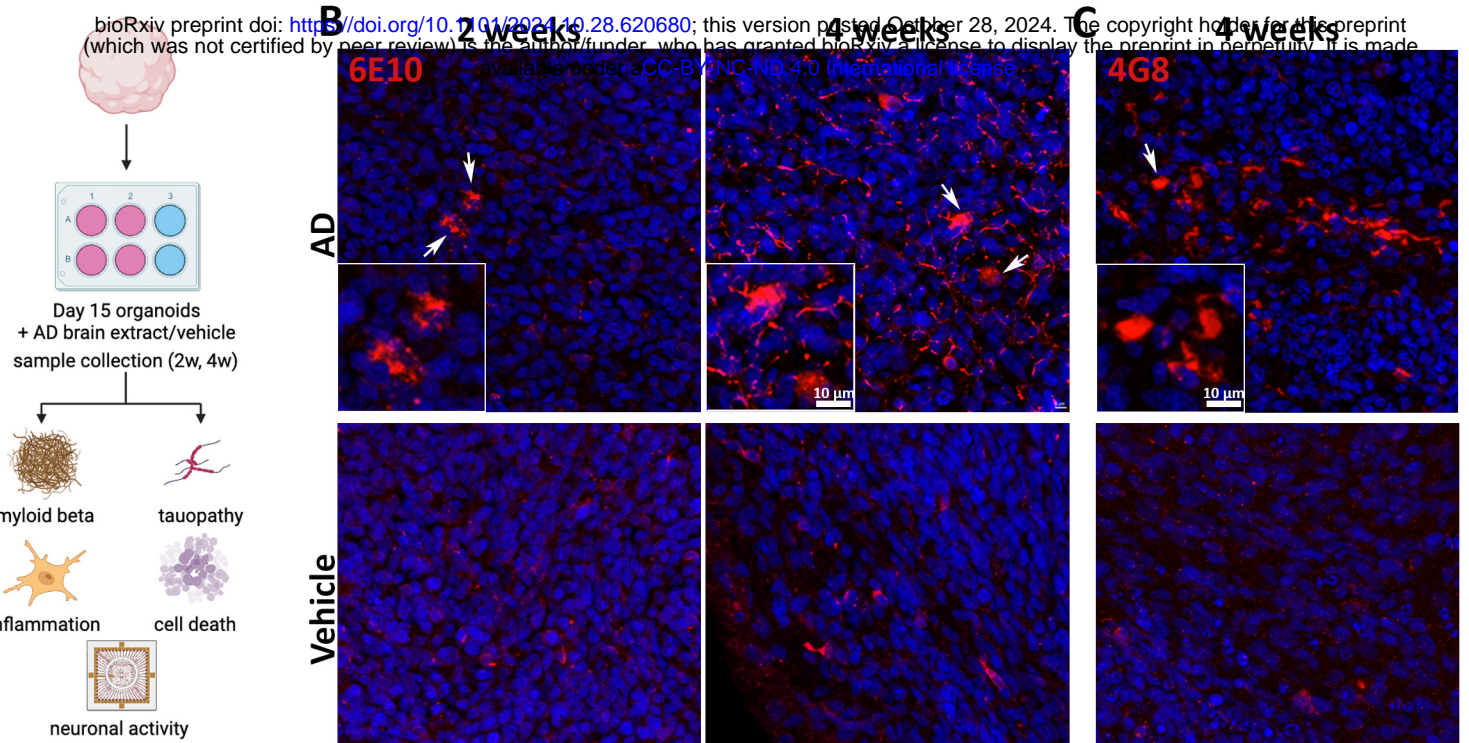
34 **Figure 5. The AD neuroimmune organoids recapitulate synapse/ neuronal loss and  
35 impaired neural activity.**

1 (A) Representatives of Homer1 staining in the vehicle and AD groups at 4 weeks post-  
2 exposure to the vehicle or AD brain extracts, respectively. Scale bar, 5  $\mu$ m.  
3 (B) Quantification of Homer1 puncta number per 2500  $\mu$ m<sup>2</sup>. n = 4 independent experiments  
4 from three hPSC lines, each experiment used one hPSC line and contained 4-6 organoids.  
5 Data are presented as mean  $\pm$  SEM. Unpaired t test with Welch's correction, \*\*p < 0.01.  
6 (C) Representatives of activated Caspase3 staining in the vehicle and AD groups at 4 weeks  
7 post-exposure to the vehicle or AD brain extracts, respectively. Scale bars, 20 or 10  $\mu$ m as  
8 indicated.  
9 (D) Quantification of the percentage of Caspase3<sup>+</sup> cells. n = 4, four independent  
10 experiments from three hPSC lines, each experiment used one hPSC line and contained 4-  
11 6 organoids. Data are presented as mean  $\pm$  SEM. Unpaired t test with Welch's correction,  
12 \*\*p < 0.01.  
13 (E) Representative of organoid attached to MEA plate. Scale bar, 300  $\mu$ m.  
14 (F) Representatives of spikes/bursts within 2 s on a single electrode in the organoids from  
15 the vehicle group or the AD group.  
16 (G) Representatives of spike raster plot generated from MEA recording raw data from the  
17 vehicle group and AD group.  
18 (H) Quantification of MEA parameters. n = 4 independent experiments from two hPSC lines,  
19 each experiment used one hPSC line and contained 4-6 organoids. Data are presented as  
20 mean  $\pm$  SEM. Unpaired t test with Welch's correction, \*\*p < 0.01, \*\*\*p < 0.001.  
21

22 **Figure 6. Anti-A $\beta$  antibody Lecanemab relieved amyloid burden in AD neuroimmune  
23 organoids.**

24 (A) Representatives of 6E10 and 4G8 staining from the vehicle group, AD group, and  
25 Lecanemab-treated group. Scale bar, 20  $\mu$ m.  
26 (B) Quantification of 6E10 and 4G8 positive area. n = 3, three independent experiments  
27 from three hPSC lines, each experiment used one hPSC line and contained 4-6 organoids.  
28 Data are presented as mean  $\pm$  SEM. One-way ANOVA, \*p < 0.05, ns represents no  
29 significance.  
30 (C) Representatives of 3D reconstructive figures showing the internalization of A $\beta$  by  
31 microglia. Organoids from the AD group and Lecanemab-treated group were stained with  
32 IBA1 and 6E10. Scale bars, 4 or 2  $\mu$ m as indicated.  
33 (D) Quantification of microglial phagocytosis of A $\beta$ . n = 3 independent experiments from  
34 three hPSC lines, each experiment used one hPSC line and contained 4-6 organoids. Data  
35 are presented as mean  $\pm$  SEM. Unpaired two-tailed t test with Welch's correction, \*p <  
36 0.05.



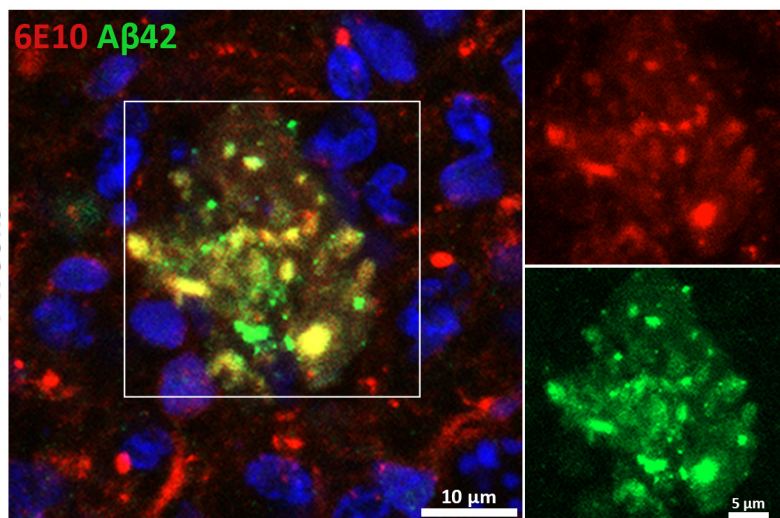
**A****B** 2 weeks**C** 4 weeks**6E10****4G8****D****Vehicle****AD****Vehicle****E****6E10 Aβ42****F****Thio-S****AD****Vehicle****6E10****Merge**

20 μm

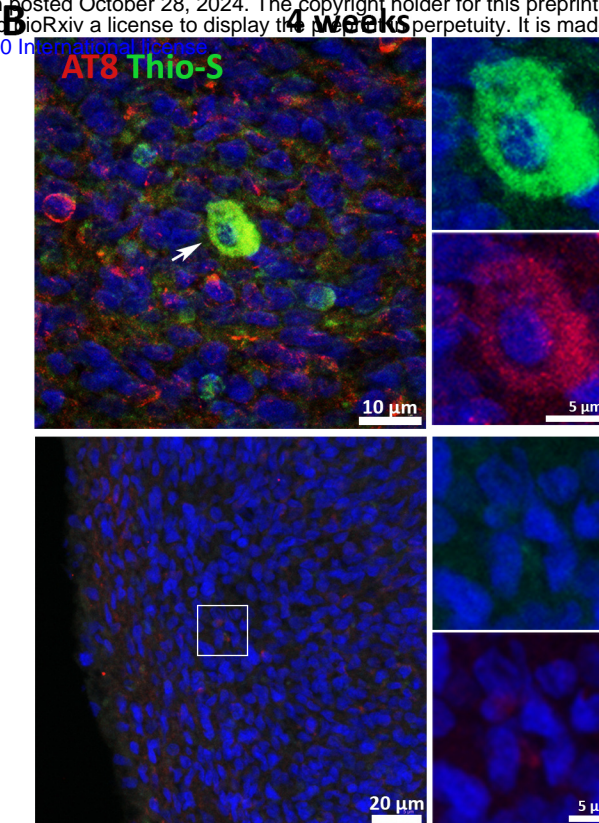
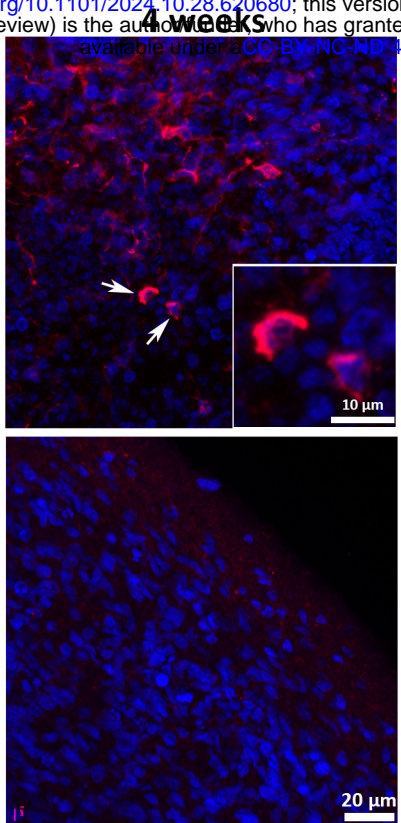
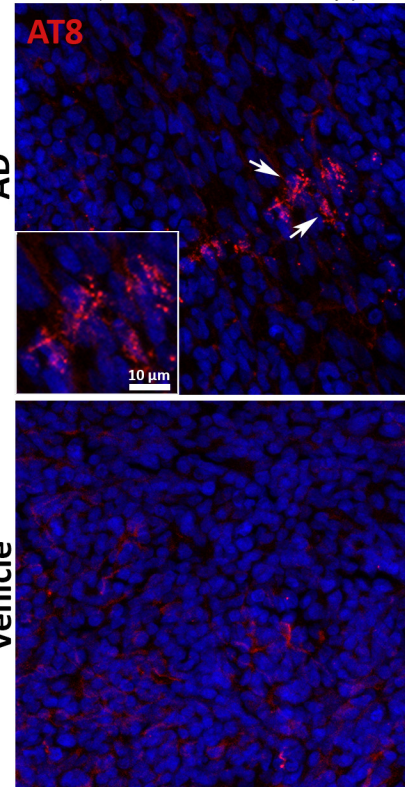
5 μm

20 μm

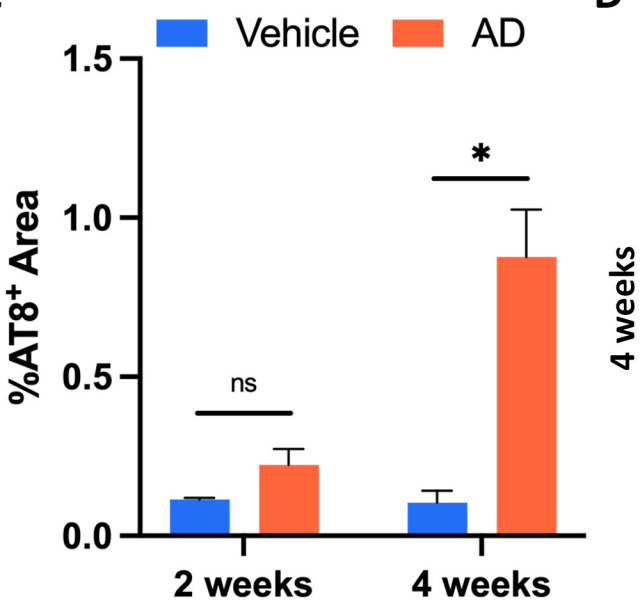
20 μm

**E****4 weeks****4 weeks**

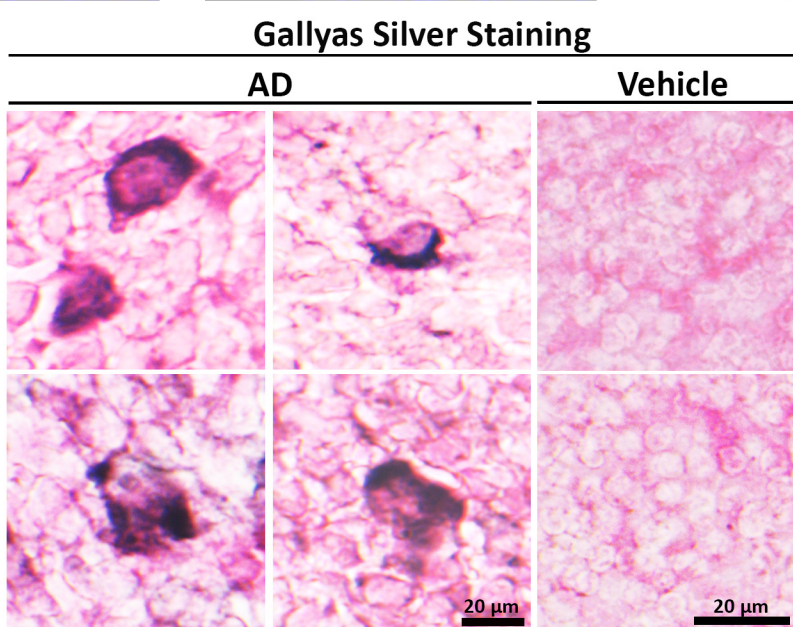
**A**

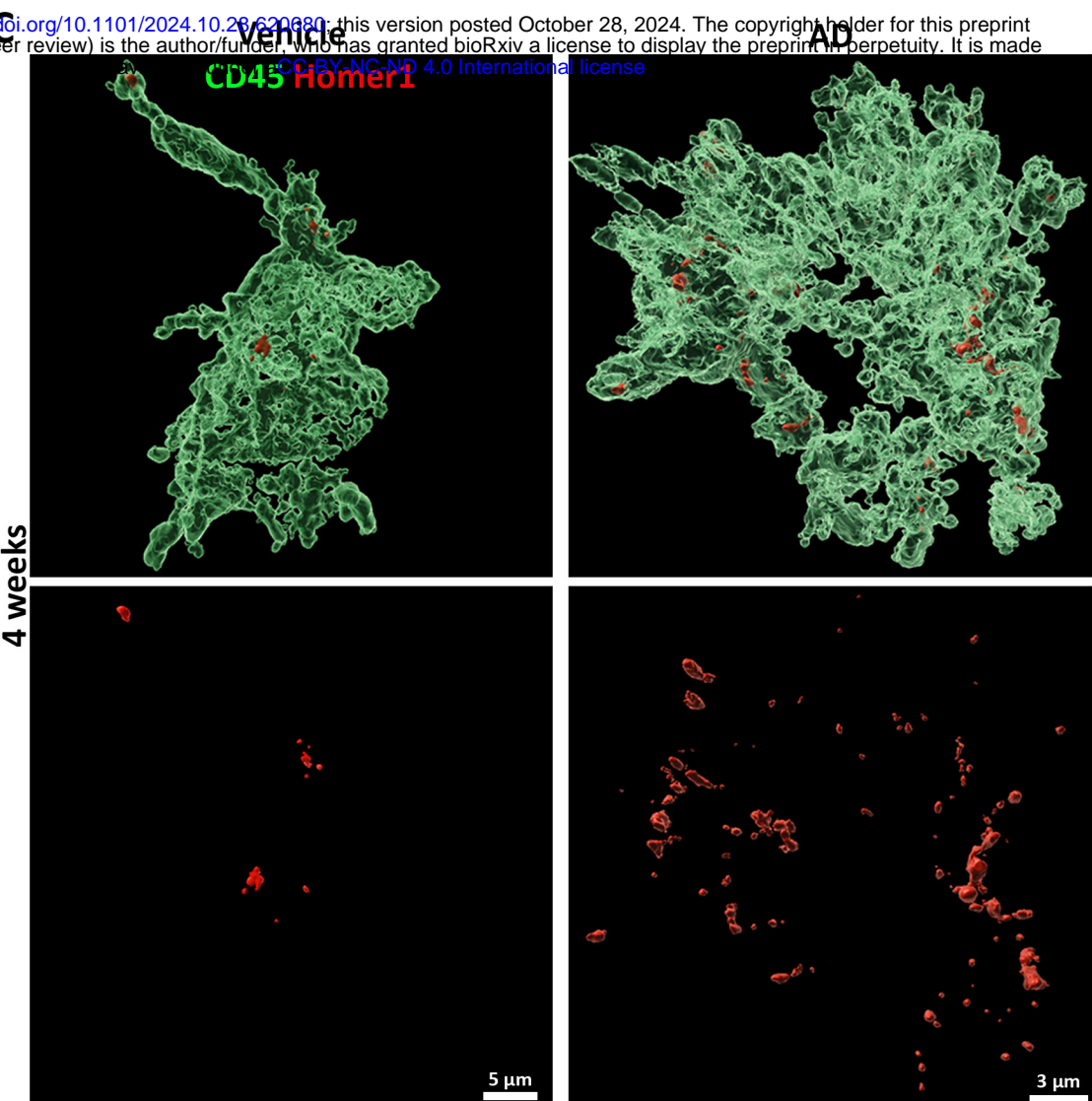
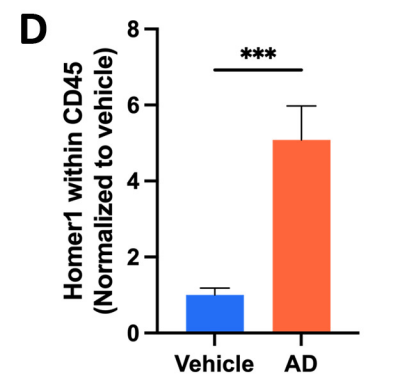
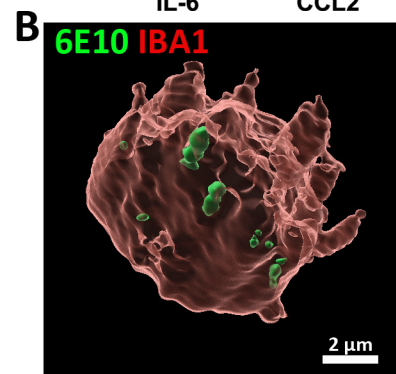
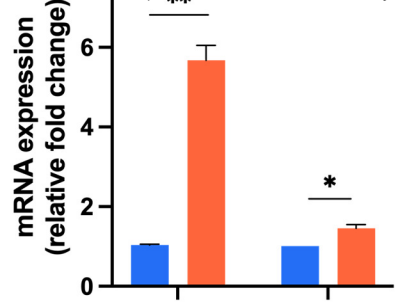


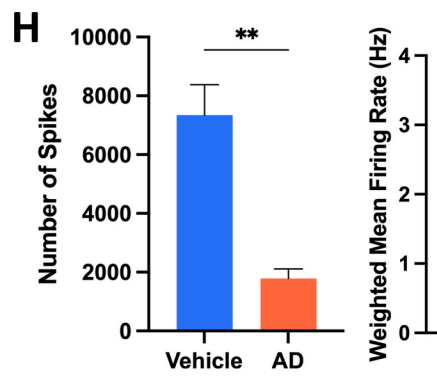
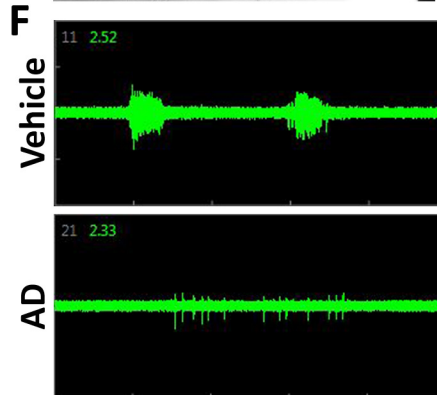
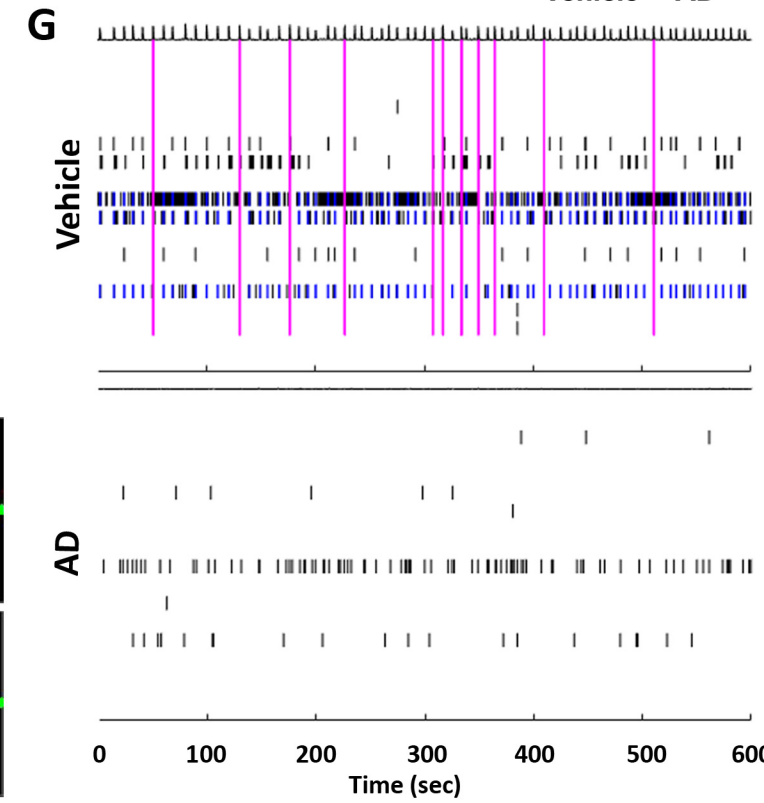
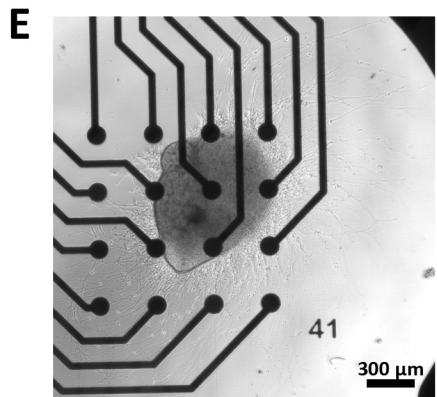
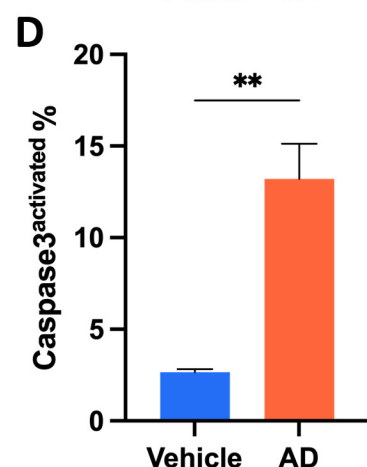
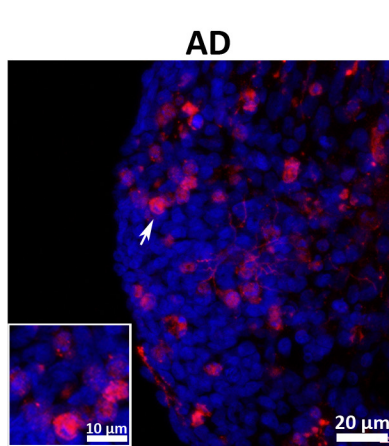
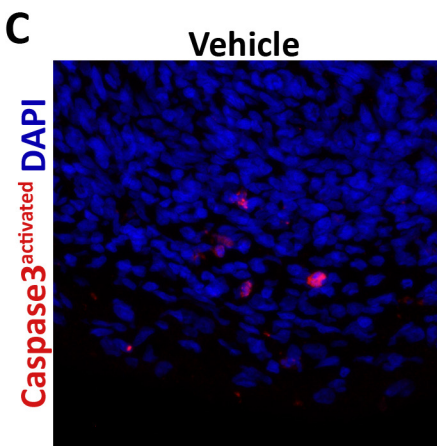
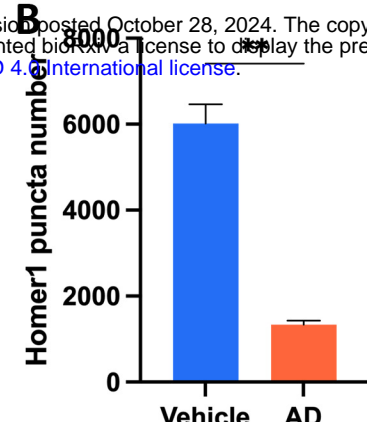
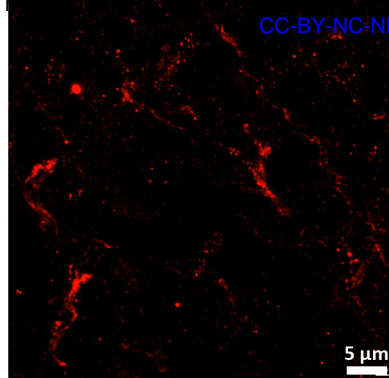
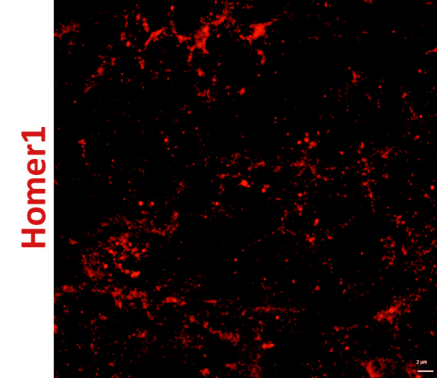
**C**

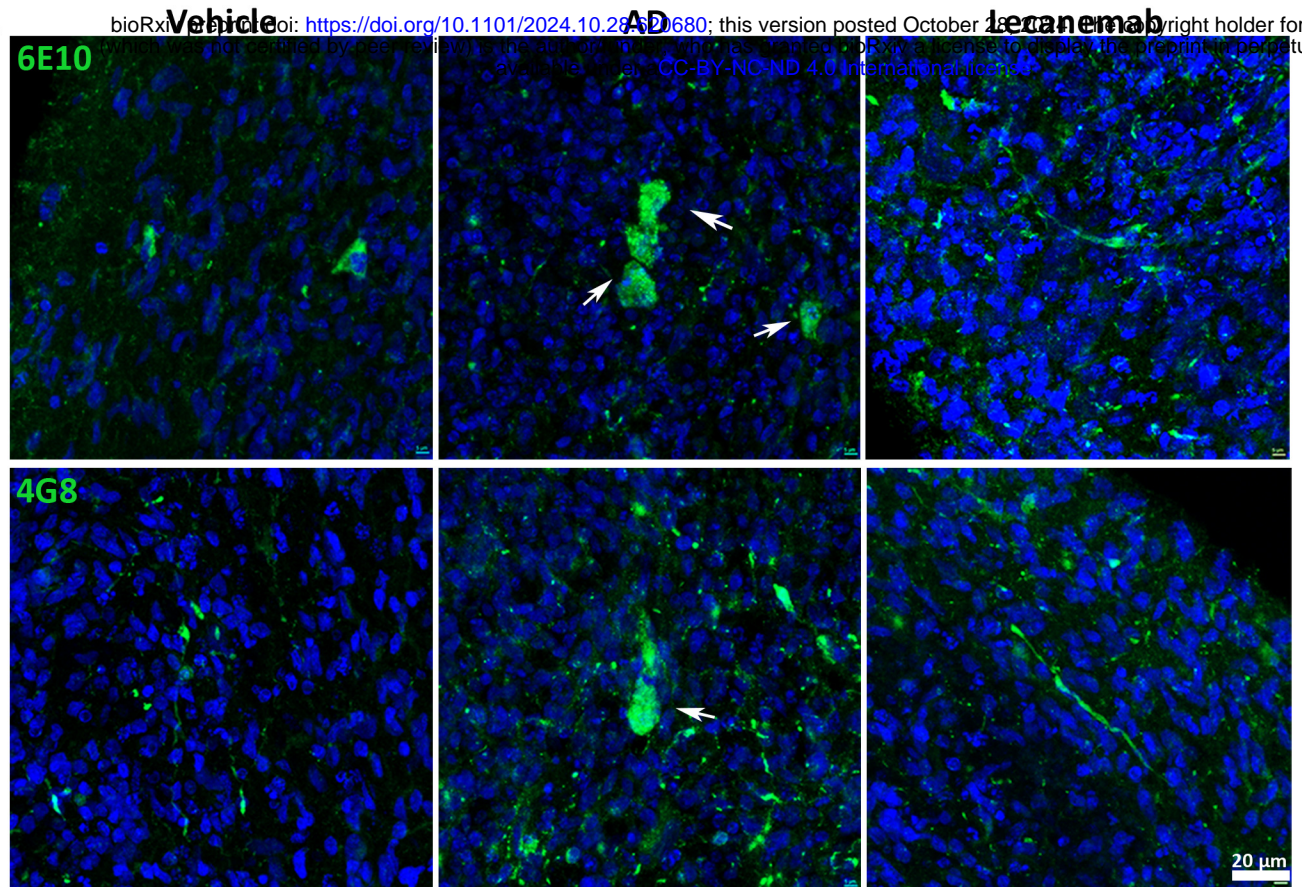
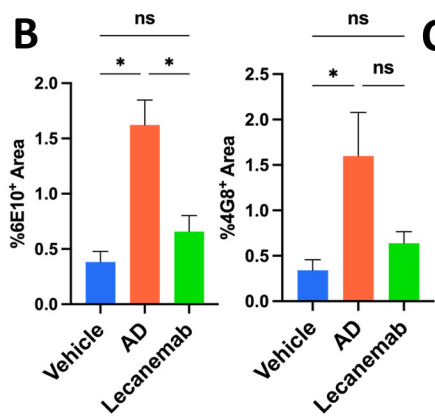
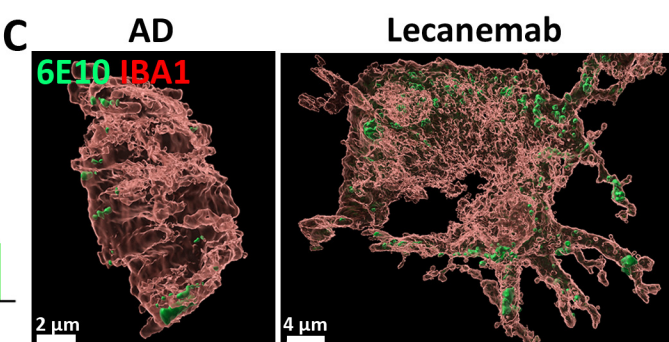


**D**







**B****C****D**